Geochemical and Hydrochemical Analysis of a Quartzite-Dolostone Bedrock Aquifer in the Central Champlain Valley, Monkton, Vermont

by

Amanda N. Fishbin

Submitted in partial fulfillment of
the requirements for the degree of
Bachelor of Arts
Department of Geology
Middlebury College
Middlebury, Vermont U.S.A.

May 2016

Fishbin, Amanda N. 2016, Geochemical and Hydrochemical Analysis of a Quartzite-Dolostone Bedrock Aquifer in the Central Champlain Valley, Monkton, Vermont: Unpublished senior thesis, Middlebury College, Middlebury, Vermont, 74p.

ABSTRACT

Previous studies have identified groundwater contamination from naturally occurring inorganic constituents in fractured bedrock aquifers in some areas of Vermont. For example, quartzites and phyllites of the hanging wall of the Hinesburg thrust fault are sources of elevated radionuclides (uranium and alpha radiation). This study aims to assess a fractured bedrock aquifer where lithology is comprised mainly of Cambrian Monkton Quartzite and Dunham Dolostone. The area is situated in the footwall of the Paleozoic Hinesburg thrust and is bisected by the Mesozoic St. George normal fault. To date, no systematic information on groundwater quality, aquifer potential or bedrock composition has been collected from this part of the Champlain Valley. Groundwater from 28 wells and bedrock from representative rock outcrops have been sampled for analysis of major and trace element composition. Water samples were collected from purged wells unaffected by water softeners.

Gross alpha radiation exceeds the Vermont Department of Health action level of 5 pCi/L in 11% (3/28) of wells tested (the level at which further testing for radium is recommended). Groundwater sampled from wells completed in the Dunham Dolostone tends to have higher alpha radiation levels than ground water from other formations. Hydrochemical data indicate that 50% of wells contain $\geq$ 2 µg/L uranium (U), 10 % contain > 5 µg/L U, and 5% contain > 10 µg/L U; notably, none exceed the Vermont U Maximum Contaminant Level (MCL) of 20 µg/L. Alpha radiation and U are positively correlated in groundwater, suggesting that U is the likely source of alpha radiation; calculations of residual gross alpha content suggest that radium (Ra) is $\leq$ 5 pCi/L in this aquifer system. Variation in reduction-oxidation potential of the aquifer system is indicated by varied abundances of manganese (Mn) and iron (Fe). Mn concentrations are >100 µg/L in 20 % of wells, and Fe exceeds 100 µg/L in 35 % of wells. In other cases, both are below detection limit. Lead (Pb) exceeds the 15.0 µg/L health standard in one well, where its concentration was 22.1 µg/L. Arsenic (As) in all wells is less than the EPA MCL of 10 µg/L; in fact, only one (at 2.5 µg/L) even exceeds 1 µg/L.

This study indicates that the Monkton Quartzite contributes lower amounts of radionuclides and other trace elements to groundwater than do the older quartzites of the Cheshire and Pinnacle Formations. One possible explanation for this difference is that well yield in the Monkton Quartzite is greater than for wells producing from the Cheshire or Pinnacle formations, implying that lower residence time of groundwater in the Monkton limits release of radionuclides into solution. Also, the Monkton is relatively undeformed relative to the Cheshire and Pinnacle, so zircons and other potential radionuclide sources in the Monkton have not been affected by shearing and grain size reduction to the extent that has been observed on the more-deformed units. This may inhibit release of radionuclides into solution.

ACKNOWLEDGEMENTS

I would first like to thank Pete Ryan for his invaluable guidance and support throughout my entire thesis process. Thanks for allowing me to bombard you with questions during our jam sessions, and for those many hours driving around Monkton. Most importantly, thank you for helping me narrowly avoid getting arrested and for debating the true identity of the bear and rabbit.

Thank you to Jon Kim for helping to organize this project with the Town of Monkton. I appreciate your support, consideration and very helpful GIS maps.

Thank you to Jody Smith for your patience and assistance in the basement of BiHall. Your flexible schedule and enthusiasm for assistance with lab techniques proved invaluable. Thank you Jeff Munroe for taking time out of your busy schedule as Department Chair to help me ignite samples and create box plots. I appreciate your excitement and willingness to assist my various thesis components.

Thank you to Jay Frater, Wendy Sue Harper, Rodger Wallace, Susan DeSimone, and Buzz Kuhns for helping to organize this project and helping me to find willing participants for this study. Without your assistance this research would not have been possible.

Thank you to Jessie Ralph and Perri Silverhart for assisting me with sample collection. I appreciate you taking time to help me fill up buckets of water, and for your excellent DJ skills.

Thank you to John Van Hoesen for providing me with a bedrock map that allowed me to find outcrops of bedrock for geochemical analysis. It proved a very helpful in my sample collection. Thank you to Andrew Nichols for collecting bedrock samples that I was later able to analyze.

Thank you to the entire Geology Department for making the 4th floor of BiHall one of the most inclusive and supportive communities at Middlebury. I have never enjoyed learning more. To the geology class of 2016 and 2016.5, I never could have made it through these past few years without you. Thank you for some hilarious banter in the field, never failing to help each other out, and endless fun. Thank you for putting up with my peer pressure. QUARTZ, QUARTZ, QUARTZ!

To my friends and family, thank you for enduring my endless nerdy geology rants. Mom, Dad, Katie, Chloe and Teddy, thank you for always helping me to sort out my irrational anxiety and for your never-ending support. To the Homestead 2014-15 crew, I will always treasure my time here and Middlebury. Thank you for your help making my time here an absolute blast filled with random adventures and amazing memories.

Thank you to the Senior Research Project Supplement, the Vermont Geological Society, and the Middlebury Geology Department for helping to fund this research without which I would not have been able to carry out this study.

TABLE OF CONTENTS

LISTING OF FIGURES

LISTING OF TABLES

INTRODUCTION

In New England, approximately 2.3 million people, about twenty-percent of the population, receive water for domestic use from private wells (EPA [B] 2015). Required testing of private wells is not mandated by the EPA (as it is for public water supplies), so most private wells are not tested for potential natural or anthropogenic contaminants. Many homeowners are unaware of the potential risks posed to their private wells, leading a significant proportion of the population to drink water of unknown quality (EPA [B] 2015).

Naturally occurring inorganic constituents, including U, radium, arsenic, and alpha radiation, have been shown to exceed recommended levels for safe drinking water in various fractured bedrock aquifers in northwestern Vermont (e.g. North 2005, Bean 2009, McDonald 2012, Ryan et al. 2013, Kim et al. 2014). These constituents pose a risk for various adverse health effects over long-term exposure at elevated levels. For instance, extended exposure to uranium can increase the risk of kidney damage. Well water that contains high levels of radioactive minerals increases concentration of radon in the air inside a home, and long-term exposure increases a person's risk of lung cancer (VDH [A] 2015). Long-term exposure to arsenic has been linked to increased risk of bladder, lung and skin cancer. Alpha radiation cannot pass through skin, however long-term ingestion of high levels of alpha radiation increases the risk of bone cancer (VDH [B] 2015). This is troubling considering that 40-50% of the population within the state of Vermont obtains water from unregulated, private wells from fractured bedrock, leaving a large portion of the Vermont population susceptible to adverse health impacts (Kim et al. 2014).

Previous research has shown that the hydrochemistry of groundwater in New England is closely related to the geochemistry of the underlying bedrock, degree of bedrock metamorphism, and groundwater residence time (Ayotte et al. 2003). More locally, research has shown elevated concentrations of naturally occurring inorganic constituents in wells in the hanging wall of the Hinesburg Thrust Fault in northwestern Vermont (Kim et al. 2014). The Town of Monkton, Vermont lies in the central Champlain Valley on the footwall of the Hinesburg Thrust Fault, and the bedrock aquifer in the region has not been fully assessed. The overall lack of information on composition, flow patterns and water quality in the Monkton region are the primary reasons for this study. Also, given the propensity of sandstone and quartzite aquifers to contain elevated radionuclides (Senior and Vogel 1995, Vengosh et al. 2009, Kim et al, 2014), this study provides and opportunity to examine groundwater composition in a roughly 3 by 4km area strongly influenced by Monkton Quartzite. The rest of the region is composed of interbedded quartzite and dolomite with minor phyllite beds, thus also providing a mean to examine dolomite influence on groundwater. The main hypothesis for this study is that the quartzite bedrock aquifer will contain elevated levels of radionuclides, while the dolostone dominated aquifer will contain lower levels of radionuclides.

BACKGROUND

I. Groundwater Flow in Bedrock Aquifers

In unconsolidated aquifers, the permeability of the aquifer is dependent on porosity and hydraulic conductivity (Fetter 2001), and groundwater presence is typically uniform throughout (Eaton et al. 2007). Bedrock aquifers, especially with interlocking crystalline grains, lack intergranular permeability (Fetter 2001). Water flow in fractured bedrock aquifers is dominated by fractures, while flow dynamics in unconsolidated aquifers is dependant on aquifer permeability. Therefore in bedrock with low intergranular porosity and permeability, faults and fractures control water flow rate and direction (Stanley 1980). Often, flow in bedrock aquifers is difficult to predict due to inconsistency of fracture patterns and density (Bense et al. 2013). This can lead to high levels of variability and water quality in well yields and water quality even over relatively short distances (Shapiro 2002).

Water quality and quantity problems exist close to the Hinesburg thrust fault. Specifically, there are elevated levels of gross alpha radiation and uranium in the hanging wall of the Hinesburg Thrust fault. In the hanging wall, Kim et al. 2014 found that 67% of wells in the Pinnacle quartzite exceeded 15 pCi/L gross alpha radiation. Uranium was shown to mirror gross alpha trends. In the Pinnacle Formation in the hanging wall, 25% of wells exceeded 20 µg/L uranium. Relatively low well yields in the Pinnacle Formation in the hanging wall were correlated with elevated levels of radionuclides (Kim et al. 2014). North (2005) found elevated levels of radionuclides in the Pinnacle and Cheshire quartzites in the hanging wall. Bean (2009) found lower gross alpha radiation

and U in the footwall, yet still found some wells with gross alpha radiation concentrations between 5-15 pCi/L.

II. Controls on Radionuclides in Sedimentary Bedrock

The bedrock characteristics and mineral composition of the bedrock aquifer can play a role in groundwater quality (Ayotte et al. 2003, Kim et al. 2014). Given the abundance of quartzite in Monkton some mineralogical and geochemical controls on gross alpha radiation for sandstone and quartzite are discussed.

Zircon

Zircon ($ZrSiO_4$) is a typical radionuclide mineral, which commonly includes U, thorium (Th), cerium (Ce) and lanthanum (La) (Nesse 2000). Zircon has the potential to contain up to 45,000 ppm U and 10,000 ppm thorium (Deer et al. 1966). Concentrations of U and Th can reach 2.6 ppm and 12.6 ppm respectively in the hanging wall. Rocks that contain detrital zircons typically have a Th:U ratio of 3:1 to 4:1. Lower Th:U ratios suggest that U is not included as part of detrital minerals, but perhaps occurs in authigenic minerals. One example of an authigenic U-bearing mineral that could be deposited in a marine environment is fluorapatite phosphorites (Banning and Rüde 2015).

Phosphorites

Phosphorites are defined as any rock containing at least 15% P_2O_5 (Blatt et al. 1980). Phosphorites are usually deposited on continental shelves in lower latitudes in the presence of nutrient-rich ocean water. The decay of the organic matter depletes oxygen in the depositional environment. In the anoxic conditions, the precipitation of carbonate

apatite is favored over calcium carbonate. The phosphorous from the dead organic matter is slowly released in the interstitial water, and saturates the water with calcium and phosphorous. The phosphorous precipitates as fine-grained apatite or replaces chert, calcium carbonate or skeletal remains through phosphatization. A change in ocean currents could create a higher energy environment in which allows for the transportation of phosphorite grains. Phosphorite grains are then included in breccias, as interbeds in shales, cherts, limestones, dolostones and mudstones (Boggs 2001). Uranium can be released from apatite crystal structure included in the bedrock during diagenesis or weathering. This mobile uranium can enter the groundwater aquifer.

Barium

Barium (Ba) can act as an important control on the availability if aqueous radium (Grundl and Cape 2006). Radium-226 and radium-228 are formed through the natural decay of uranium-238 and thorium-232, and Ra is relatively soluble (Zhang et al. 2014). The co-precipitation of barium and sulfate to form barite ($BaSO_4$) and carbonate to form witherite (Ba, Ra)CO_3 can sequester Ra, thus decreasing As in groundwater (Reimann and de Caritat 1990, Grive et al. 2007). Sequestration occurs with the formation of barite due to the rapid barite nucleation rate, identical charges and similar ionic radii of Ra^{+2} and Ba^{+2} (Zhang et al. 2014). The low solubility of barite and witherite can limit dissolved Ra levels in groundwater (Reimann and de Caritat 1998). One possible introduction of barium and phosphates into the groundwater system could be through mineral weathering. For example, Ba^{+2} can replace potassium or calcium in feldspars (Deer et al. 1966).

III. EPA Drinking Water Standards

The Safe Drinking Water Act includes the requirement that the EPA identifies and lists unregulated contaminants. The EPA must regularly publish a list of contaminants, and decide whether to regulate at least five of those identified contaminants (EPA [A] 2015). If the EPA decides to regulate a contaminant, it sets National Primary Drinking Water Regulations to legally apply to public water systems (EPA 2014, EPA 2015). These maximum contaminant levels are established to protect public health by setting a limit on drinking water contaminants (EPA 2014). If the EPA chooses not to regulate a contaminant, it can develop a health advisory. Health Advisories are non-enforceable limits, which are intended to serve as a guide at the federal, state and local levels. The Safe Drinking Water Act mandates the EPA to review all National Primary Drinking Water Regulations every six years. Every six years, new data, information and technology are evaluated to determine if revisions must be made to maximum contaminant levels to improve protection of public health (EPA 2015). Although maximum contaminant levels and health advisories are not legally enforced on private wells, they can be used as a standard for health. The EPA maximum contaminant levels and health advisories for certain sources of groundwater contamination are listed in Table I.

Table I. Maximum contaminant levels and health advisories for pertinent drinking water contaminants set by the EPA in public water sources (EPA [C] 2015, VDH 2014).

Contaminant	EPA Maximum Contaminant Level	EPA Health Advisory
Arsenic	10.0 µg/L	--
Lead	15.0 µg/L	--
Manganese	--	300.0 µg/L
Radium 226 and Radium 228 (combined)	5.0 pCi/L	--
Uranium	20.0 ppb	--

PREVIOUS WORK

I. Research in Vermont

Kim and Becker (2001) were the first to identify bedrock as the source of elevated levels of radioactivity in drinking water wells for the St. George Trailer Park in northwestern Vermont. Research indicates that the drinking water for the St. George Trailer Park is derived from a well in the hanging wall of the Hinesburg Thrust Fault, which is composed of the Fairfield Pond, Pinnacle and Cheshire formations (Kim and Becker 2001).

Fault systems are known to play an important role on groundwater hydrochemistry (Stanley 1980, Favorito 2014, Seaton and Burbey in Kim et al. 2014). Mapping bedrock and groundwater chemistry indicates that the dominant control on the composition of groundwater is the geochemical signature of the bedrock (Kim et al. 2014). Previous studies have shown that the hanging wall of the Hinesburg thrust in the eastern part of the Champlain Valley contains high levels of naturally occurring radioactivity, $Na^{+}K$-Cl, Ba and Sr, and high concentrations of Ca-Mg-HCO_3 and alkalinity. This includes elevated levels of gross alpha radiation and arsenic (Kim et al. 2014). Previous research has also found some evidence of elevated levels of gross alpha radiation in wells producing from the Monkton Quartzite, the bedrock formation that dominates the study region (Bean 2009). Previous research also suggests that the Hinesburg and St. George faults are responsible for radionuclide and trace metal groundwater contamination in the towns of Hinesburg and St. George (Kim and Becker 2001). These patterns are concerning for the regions in the footwall of the Hinesburg Thrust Fault (Kim et al. 2014).

II. Other Regions with High Radioactivity in Groundwater

Research in regions outside of Vermont indicates that clastic units can be sources for elevated radioactivity in groundwater. In addition, metamorphosed sandstones and mudstones are often elevated in radioactive constituents (Kim et al., 2014). Most often, intrusive igneous rocks, not crystalline metasedimentary rocks, contaminate groundwater (Senior and Vogel 1995). Radionuclide-bearing minerals, including zircon, apatite, sphene, and monazite, are only altered under high-grade metamorphism or deformation. Therefore, because they are relatively stable, these minerals often become concentrated through sedimentary processes such as erosion and deposition (Senior and Vogel 1995). This association may be significant because the Monkton Quartzite Formation dominates the bedrock aquifer in the western half of Monkton.

Senior and Vogel (1995) examined the Lower Cambrian Chickies Quartzite Formation in southeastern Pennsylvania for sources of radium in groundwater. The Chickies Formation, comprised of a basal metaconglomerate, quartzite and slate, is similar in age and composition to the Monkton Quartzite Formation. Like the Monkton Quartzite, the Chickies Quartzite is in depositional contact with Cambrian to Ordovician dolomite and limestone. Quartzite in the Chickies Formation contains elevated levels of uranium and thorium, similar to concentrations found in previous studies in Hinesburg and St. George. High concentrations of barium were correlated with low pH, low alkalinity and low silica content. Senior and Vogel suggest that radionuclides from the Chickies Formation are introduced to the groundwater through a radium parent isotope. Radium isotopes are naturally occurring radionuclides part of the U-238 and Th-232

decay series. U and Th are contained in sandstone and quartzite in detrital primary minerals and in secondary minerals (Senior and Vogel 1995).

A study by Vengosh et al. (2009) reports high levels of naturally occurring radium in Jordan, where the Disi aquifer is composed of Cambrian to Ordovician sandstone. It is suggested that radium groundwater activity is controlled by the radioactive decay of the parent isotopes (U and Th) on aquifer solids, decay of dissolved radium isotopes and adsorption of dissolved radium on solid surfaces (Vengosh et al. 2009).

GEOLOGIC HISTORY OF STUDY SITE

I. Bedrock Geology

Various bedrock units underlay the region within the geographic confines of the Town of Monkton, Vermont (Figure 1). The major rock formations were deposited on the passive Laurentian continental margin of the Iaptus Ocean from the early to late Cambrian to the Middle Ordovician (Kim et al. 2014).

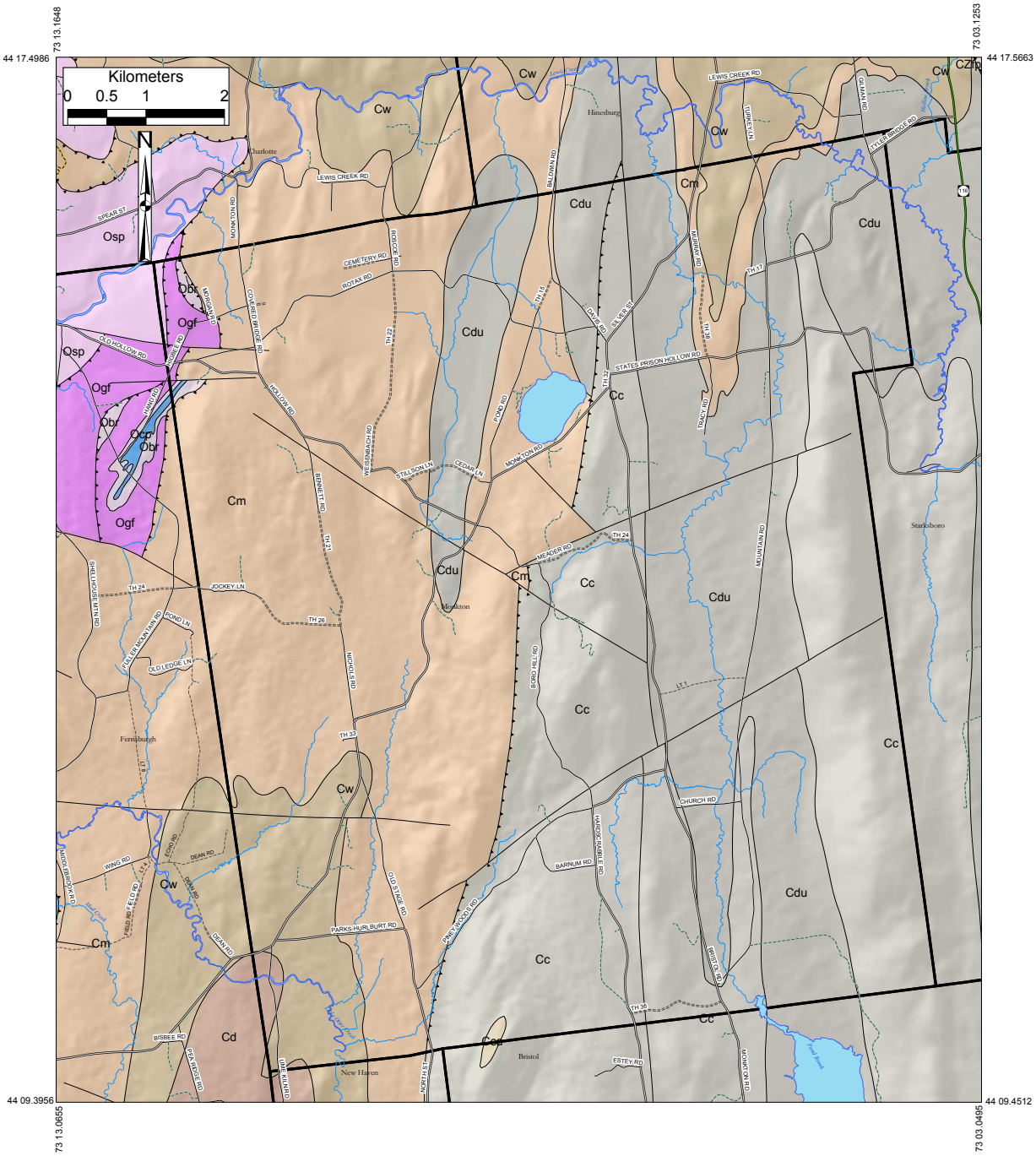

Figure 1. Geologic map of the study section. The black outline is the town boundary of Monkton, VT. Cc is Cheshire Quartzite, Cdu is Dunham Dolostone, Cm is Monkton Quartzite, Cw is Winooski Dolostone, Ogf is the Glens Falls Limestone and Obr is the Black River Group. Map courtesy of Jon Kim.

Mount Holly Complex

The Mount Holly Complex does not outcrop in the region, but is assumed to lie beneath the area at depth. The closest outcrop of the Mount Holly Complex occurs at the gorge of the Middlebury River in East Middlebury, Vermont. The outcrop comprises of complex, heterogeneous group of contorted and re-crystallized quartz-feldspar-biotite granulite (Ogden 1969). The formation is dominated by granites and gneisses (Ratcliffe et al. 2011).

Mendon Formation

The Mendon Formation does not outcrop in the region, but is assumed to underlie the Cheshire Quartzite. It is a complex unit dominated by conglomerate, quartz-muscovite schist, porphyroblastic albite-quartz-biotite-muscovite schist, and quartz-chlorite-muscovite schist (Ogden 1969).

Cheshire Quartzite

The Cheshire Quartzite Formation overlies the Mendon Formation. It is usually composed of massive, white quartzite. The lower portion of the formation is exposed in Monkton and differs from other outcrops observed in adjacent regions. The outcrops in Monkton are light gray and brown in color, porous and exhibit bedding structures. The quartzite is interbedded with argillaceous and schistose layers. The Cheshire Quartzite in the Monkton region underwent a high degree of re-crystallization (Ogden 1969).

Dunham Dolomite

The Dunham Dolomite overlies the Cheshire Quartzite Formation. The outcrops in the Monkton, Vermont region are composed of mostly siliceous, buff-weathered dolomite with irregularly distributed well-rounded sand grains. Thicker beds of quartzite occur near the contact with the Monkton Quartzite Formation (Ogden 1969).

Monkton Quartzite

Outcrops of the Monkton Quartzite Formation in Monkton are red in color and massive with interbeds of reddish purple slate. Monkton Quartzite beds dip 50-70 degrees to the east. Ripple marks, mud cracks and cross beds are common. Monkton Quartzite forms resistant ridges in the throughout the region (Ogden 1969).

Kaolin Deposits

Kaolin deposits are found in fractures and distinct layers (kaolinized phyllite beds) within the Cheshire Quartzite Formation (Ogden 1969, Stanley 1980, Nichols 2001). The kaolin deposits in Monkton differ from other kaolin deposits in Vermont, which occur as surficial deposits above bedrock. The kaolin deposits are associated with iron-manganese deposits (Stanley 1980).

Glacial Deposits

Bedrock in the Monkton region is overlain by glacial deposits composed of sand and gravel, mostly in irregular masses (Ogden 1969). There are no known glacial

deposits significantly thick or extensive enough in Monkton to serve as a surficial aquifer.

II. Structural Geology

Major thrust faults and folds characterize the bedrock underlying and exposed within Monkton (Stanley 1980). During compression associated with the Ordovician Taconic orogeny, the Hinesburg thrust fault formed at depth as a ductile fault. It is comprised of biotite-grade quartzites and phyllites in the hanging wall and weakly metamorphosed carbonates, shales and quartzites in the footwall. The strata and fault system were further deformed by compression associated with the Acadian Orogeny during the Devonian period. Mesozoic extensions caused fracturing and faulting (Kim et al. 2014). The Town of Monkton lies in the footwall of the Hinesburg thrust fault and in the hanging wall of the Champlain thrust fault (Figure 2), and is bisected by the north-south St. George normal fault (Ogden 1969, Stanley 1980).

Fracture fabrics increase closer to major faults (particularly where they intersect) and major folds of the Hinesburg synclinorium (Stanley 1980). These north-south oriented fractures might have important implications for hydrogeology. The complex groundwater flow patterns ultimately shape the transport of naturally occurring inorganic contaminants (Kim et al. 2014).

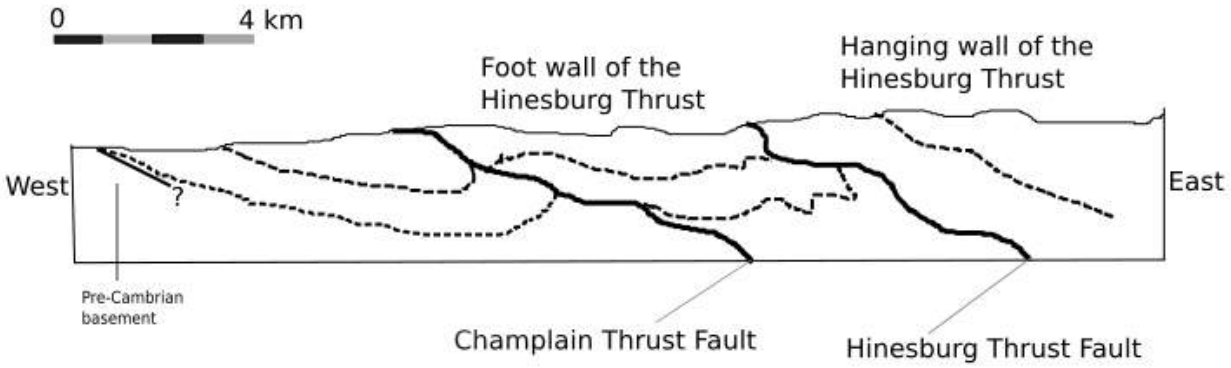

Figure 2. Simplified cross section of the Hinesburg Thrust Fault, the Champlain Thrust Fault, and the regional structural trends. Modified from Kim et al. 2011 and Filoon 2012.

PURPOSE

The bedrock underlying Monkton is dominated by crystalline bedrock with little or no porosity; as a result, fractures, bedding planes or other lineations play an important role in the hydrogeology of the region. Groundwater flow is anisotropic (hydrologic conductivity differs in the horizontal and vertical direction). As a result, it is difficult to predict flow and yield within a bedrock aquifer. A lack of understanding of groundwater flow is problematic, because previous research that documents elevated radionuclides in adjacent regions and with similar bedrock types indicates that Monkton might host groundwater with concern to human health standards (North 2005, Bean 2009, McDonald 2012, Kim et al. 2014). The chemical quality of the groundwater in Monkton is likely dependant on the geochemistry of the bedrock in the region. It is therefore important to gain a better geochemical and hydrochemical understanding of the region and bedrock aquifer.

Quartzites in the hanging wall of the Hinesburg Thrust fault cause elevated levels of gross alpha radiation and uranium in groundwater that exceed safe drinking water standards. Quartzite aquifers in the footwall of the Hinesburg thrust fault (such as the Monkton Quartzite Formation) have not been fully assessed for composition or aquifer potential. It is possible the Monkton Quartzite aquifer poses similar drinking water issues to the quartzites of the hanging wall. Sediments of the Monkton Quartzite likely had a similar source to the Cheshire Quartzite Formation (which is associated with elevated levels of radionuclides and uranium in the hanging wall of the Hinesburg Thrust fault), and both were deposited on the Laurentian passive continental margin (Kim et al. 2014).

This study will examine whether the Monkton Quartzite Formation also contains elevated radionuclide levels.

Kaolin deposits in Monkton appear to have a hydrothermal origin (Nichols 2001). They occur at along the St. George fault and might influence groundwater composition, but have not been assessed for trace elements. The kaolin in the region is known to be associated with iron-manganese deposits, further implying a potential trace element association (Stanley 1980). Geochemical and hydrochemical analysis will examine the potential impact of iron-manganese deposits on water quality.

Carbonate bedrock aquifers generally have higher permeability than crystalline silicate-dominated bedrock aquifers. Higher permeability of carbonates in areas previously studied in the footwall of the Hinesburg thrust fault are associated with relatively low levels of radionuclides and higher well yields than the hanging wall (Kim et al. 2014). However, carbonate aquifers in the footwall remain poorly understood. This study will provide an additional opportunity to examine dolostone aquifer characteristics.

METHODS

I. Hydrochemical Analyses

Groundwater Collection

Twenty-eight water samples were collected from private wells in Monkton, VT. Efforts were made to include a wide geographic spread in the study region as well as samples of water in different bedrock units. Property owners gave permission for samples collected from each well. In order to ensure anonymity of property owners, a sample ID scheme including the date and number was used. All groundwater samples collected were unfiltered and were not affected by water softeners. Wells were located using GPS.

Water was run through a hose, spigot, or sink (depending on individual property water systems) into a bucket, which was used as a flow chamber. A YSI multi-probe was inserted into the bucket to measure temperature, conductivity, dissolved oxygen, and oxygen-reduction potential (Figure 3). Water was allowed to run until the YSI multi-probe measurements stabilized, indicating water was coming directly from the well. YSI multi-probe measurements were recorded. For each site seven acid-rinsed sample bottles and one sterilized whirl-pack bag were each rinsed three times, and then filled with water from the source. The samples were placed in a cooler, and either directly delivered to laboratories for testing or placed in a refrigerator and delivered within 30 hours of sampling. From each site, six samples were brought to the Department of Environmental Conservation (DEC), one sample was brought to the Vermont Department of Health (VDH), and one sample was brought to Middlebury College.

Figure 3. Set up for YSI probe measurements.

Groundwater Analyses

The DEC completed hydrochemical analyses by ICP-MS and ion chromatography (IC). Analyses were completed to determine chemical groundwater constituents, including trace metals, major elements and anions (Kim et al. 2014). ICP-MS analyses

were duplicated at Middlebury College. The pH of each sample was analyzed using a Hach Sension 1 probe at Middlebury College. The Vermont Department of Health (VDH) analyzed one sample from each site for gross alpha radiation using EPA method EERF 00-02. Gross alpha radiation is a measurement of total aqueous radioactivity due to the decay of alpha-emitting elements.

II. Geochemical Analyses

Bedrock Collection

A total of 18 bedrock samples representative of the study area were used in this study. Fourteen of these bedrock samples were collected in the fall and winter of 2015. The remaining four samples were collected by Andrew Nichols in 2001, but were never geochemically analyzed. A list of bedrock samples analyzed in this study is presented in Appendix I.

Bedrock Sample Preparation and Analyses

Bedrock samples were analyzed using X-ray diffraction (XRD), X-ray fluorescence (XRF) and inductively coupled plasma-mass spectrometry (ICP-MS) at Middlebury College. Each bedrock sample was first cleaned, and then cut using a diamond tipped rock saw. Samples were then powdered using a jaw-crusher and shatter box. For XRD analyses, a mixture of 3.6 g of the powdered sample and 0.4 g of ZnO were prepared. ZnO was included as an internal standard. For XRF and ICP-MS analyses, all samples were placed in a LECO instrument for 60 minutes at 1000 ºC to burn off all organic matter. For XRF analysis, 0.8000 g (+/- 0.0010 g) of ignited sample

and 8.000 g (+/- 0.005 g) of $Li_2B_4O_7/LiBO_2$/Lil (11.90/21.90/0.17) (C-0650-70) were fluxed. For carbonate rich samples, 0.6000 g (+/- 0.0010g) of ignited sample and 6.000 g (+/- 0.005g) of $Li_2B_4O_7/LiBO_2$/Lil (11.90/21.90/0.17) (C-0650-70) were fluxed. Whole rock analyses were completed using the ICP-MS for both trace elements and rare earth elements. For both trace and rare earth element analysis, a 100x sample solution was created by mixing 0.2000 g (+/-0.0005 g) of sample and 1.800 g (+/-0.005g) of flux ($LiBO_2$/LiBr (98.50/1.50)(C-0610-66)). The samples were then fluxed in the Claisse Fluxer, and the fused, molten sample was dissolved in 70 mL 5% HNO_3 then diluted to 100.0 mL. For trace element analysis 5 mL of the 100x stock solution and 2 mL of the 1 ppm Traces internal standard solution (Rh, In, Re, Bi) were made up to 100 mL with 5% nitric acid. For rare earth element analysis (Cs, Rh, Re) 10 mL of the 100x stock solution and 2 mL of the 1 ppm Traces internal standard solution were made up to 100 mL with 5% nitric acid.

III. Well Yields

All well yield data were collected using the "Well Completion Report Searchable Database" provided by the Drinking Water and Groundwater Protection Division of the Vermont Department of Environmental Conservation. Since 1966, Vermont licensed drillers have been required by the state to submit well logs to the state (VT DEC 2003). This database provides data including well location, tag number, total depth of well, yield of well, and a description of changes in lithology with depth. This dataset was used to determine yields of wells located in quartzite bedrock and dolostone bedrock.

RESULTS

I. Hydrochemical Data

Gross alpha radiation exceeds the Vermont Department of Health action level (≥5 pCi/L) in about 11% (3/28) of wells tested in this study. Elevated levels of gross alpha radiation occur in wells located in the Dunham Dolostone and Winooski Dolostone. About 54% (15/28) of wells contain greater than or equal to 2 µg/L uranium, however none exceed the maximum contaminant level of 20 µg/L. Manganese was elevated (greater than 100 µg/L) in 14% (4/28) of wells located in the Dunham Dolostone. Manganese exceeded the maximum contaminant level (greater than 300 µg/L) in 7% (2/28) of wells in the Monkton Quartzite. Iron was greater than 100 µg/L in 32% (9/28) of wells. Lead exceeded the maximum contaminant level (>15 ppb) in 1 well located in the Cheshire Quartzite. Manganese in the Monkton Quartzite showed a wide range of variability. Out of the 28 wells tested, 2 Monkton Quartzite wells contained levels of manganese that exceeded the EPA health advisory standard (300 µg/L). Radium did not exceed the maximum contaminant level (5 pCi/L) in any wells tested. In addition, arsenic does not exceed the EPA maximum contaminant level in any wells tested (10 µg/L); only one sample (at 2.5 ppb) exceeded 1 ppb arsenic (Appendix II). The map in Figure 4 shows the location of all wells tested, and indicates wells that exceeded health standards.

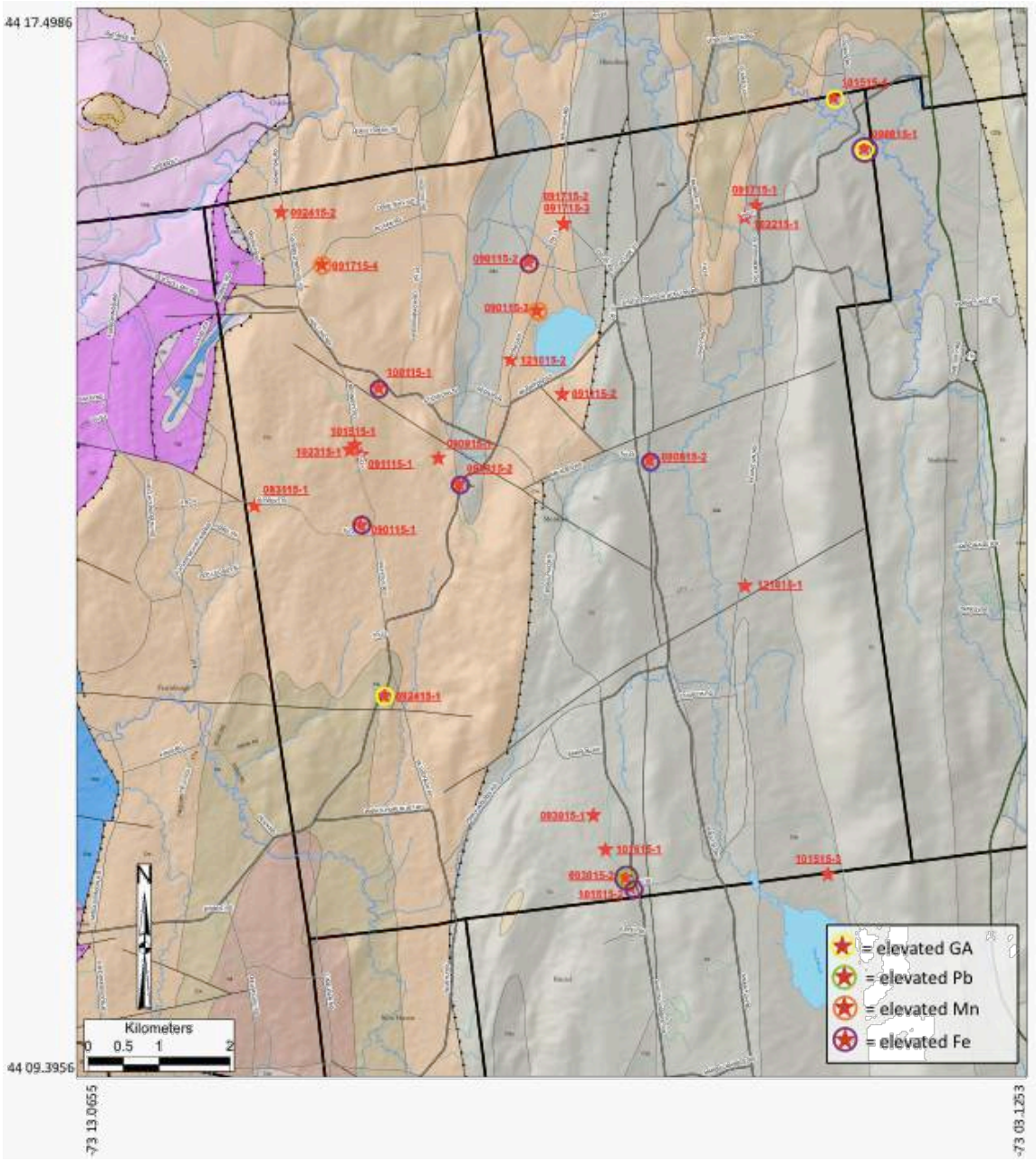

Figure 4. Bedrock map with all 28 well testing sites. Wells with elevated levels of gross alpha (GA), lead (Pb), manganese (Mn) and iron (Fe) are indicated.

A piper plot of the groundwater samples from Monkton shows the chemical classification shows the groundwater has a dominantly Ca-Mg bicarbonate signature.

Water samples taken from Cheshire Quartzite bedrock wells have a slightly lower bicarbonate signature (Figure 5).

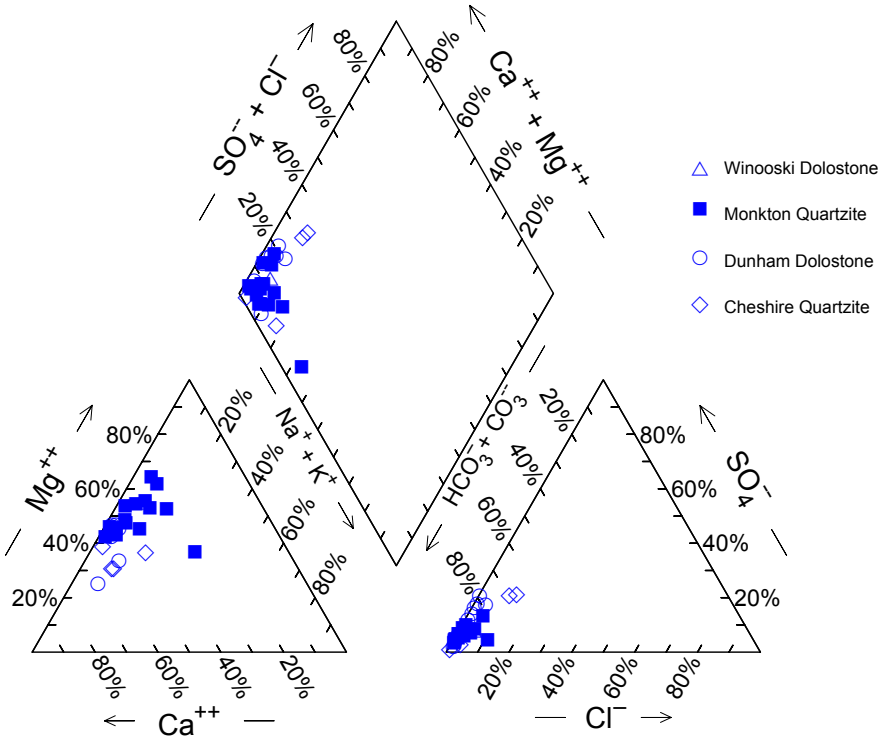

Figure 5. Piper plot of groundwater samples from Monkton.

There is a strong positive correlation between U and gross alpha radiation in bedrock samples in Monkton (R^2= 0.86) (Figure 6).

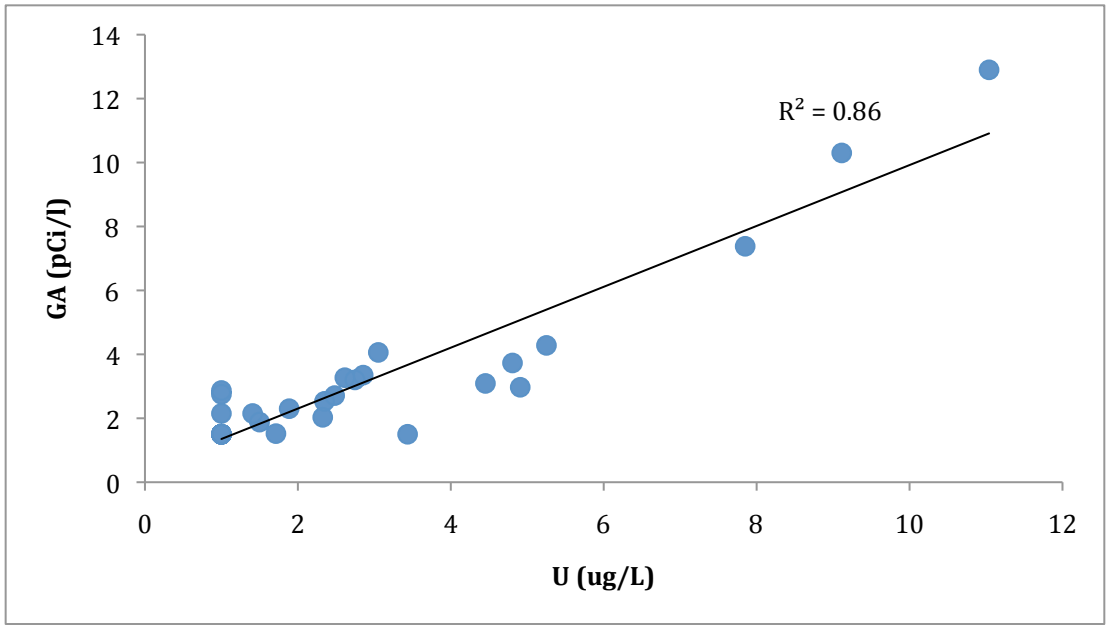

Figure 6. U concentrations versus gross alpha radiation concentration groundwater samples in Monkton. There is a strong positive relationship between U and gross alpha radiation.

A full listing of all parameters tested and hydrochemical data can be viewed in Appendix II.

II. Lithology in the Town of Monkton, VT

There is diversity in lithology within each bedrock formation in the study area. Outcrops observed of the Dunham Dolostone formation in Monkton are quartz rich (Appendix III). Samples 112215-C1, 112215-C2 and 112215-D were collected from a quartzite rich bed in the Dunham Dolostone Formation with medium beds (Figures 7 and 8). The bedrock is relatively impermeable in terms of intergrains, but fractures and bedding planes would allow space for water to flow through. Contrastingly, other sections of the Dunham Dolostone Formation in the region are composed of very sheared, phyllitic bedrock (Figure 9). These sheared, phyllitic layers with low permeability have

the capacity to hinder groundwater flow. Samples 112215-A, 12215-B1 and 112215-B2 were collected from such phyllitic, sheared Dunham Dolostone bedrock outcrops. Differences in bedrock aquifer lithology and permeability might impact yield, residence time and radionuclide levels in Monkton, as well as explain differences in radionuclide levels between this area and other regions in the footwall of the Hinesburg thrust fault.

Figure 7. Quartzite-rich, medium bedded Dunham Dolostone outcrop.

Figure 8. Quartzite-rich, medium bedded Dunham Dolostone outcrop.

Figure 9. Phyllitic and sheared Dunham Dolostone outcrop.

Diversity was also observed within outcrops of the Monkton Quartzite formation outcrops. Some outcrops have large to massive beds with large fractures (Figure 10), while other outcrops in the region are more phyllitic and massive, with fewer visible

fractures (Figure 11). The more phyllitic and massive sections of Monkton Quartzite are less permeable, and provide less opportunity for water flow compared to the thick-bedded outcrops. It is also likely that variation of lithology within the region allows for variation in yield, residence time and radionuclide levels.

Figure 10. Outcrop of Monkton Quartzite with thick beds and fractures.

Figure 11. Outcrop of massive, phyllitic Monkton Quartzite.

III. Bedrock Geochemical Data

Average Monkton Quartzite and Dunham Dolostone whole rock geochemistry shows that both have zirconium (Zr), barium (Ba), and thorium (Th) levels that exceed average crustal abundances (sandstone and carbonate respectively). The Dunham Dolostone average concentration of U is lower than average crustal abundances for carbonates, while the Monkton Quartzite has a higher average concentration of U is lower than average crustal abundances for sandstones. The Monkton Quartzite has an average Th concentration of 7.6 ppm, which is lower than the Pinnacle and Cheshire Quartzite average concentration (12.6 ppm) (Kim et al. 2014). The Monkton Quartzite also has lower average U concentration (2.0 ppm) than the Pinnacle and Cheshire Quartzite (2.6 ppm) (Kim et al. 2014) (Tables II and III).

Table II. Selected geochemical data. Full listing of geochemical data available in Appendix III.

	SiO_2 (%)	TiO_2 (%)	Al_2O_3 (%)	Fe_2O_3 (%)	MnO (%)	MgO (%)	CaO (%)	Na_2O (%)	K_2O (%)	P_2O_5 (%)	75As [ppm]	137Ba [ppm]	63Cu [ppm]	208Pb [ppm]	88Sr [ppm]	232Th [ppm]	238U [ppm]	90Zr [ppm]
082815-1A	69.21	0.63	14.25	4.63	0.004	0.91	0.43	0.12	9.70	0.17	0.67	1021.28	14.61	18.02	88.92	5.69	2.29	437.96
082815-1B	98.83	0.35	1.06	0.59	ND	0.27	0.17	ND	0.86	0.17	0.44	93.96	19.54	9.10	9.27	12.24	1.42	501.01
082815-1C	73.92	0.63	6.79	2.28	0.105	4.41	7.19	ND	4.71	0.16	0.50	470.37	22.59	15.33	91.87	5.35	1.77	588.01
082815-1D	85.12	0.75	3.30	1.62	0.131	3.19	4.93	ND	2.50	0.20	0.78	371.50	20.85	17.75	61.22	9.74	2.12	686.49
082815-2A	81.33	1.02	8.59	3.06	0.003	0.59	0.47	ND	5.49	0.29	1.41	569.73	19.64	27.02	58.94	8.40	2.79	883.65
082815-2B	79.83	0.63	3.46	1.83	0.194	4.93	7.71	ND	2.33	0.21	0.25	272.89	16.62	17.78	87.08	7.44	1.72	788.37
082815-3A	63.27	0.89	18.03	3.71	ND	1.74	0.34	0.09	11.18	0.25	0.79	955.55	9.04	42.75	64.12	7.23	2.60	684.96
082815-3B	90.83	0.59	3.97	2.03	0.330	0.28	0.23	ND	2.97	0.23	2.08	444.47	18.49	16.71	33.63	4.65	1.95	635.80
112215-A	66.23	0.93	17.65	2.11	0.018	0.78	0.46	0.26	11.06	0.13	7.02	1125.55	14.58	20.57	86.82	9.95	2.64	510.35
112215-B1	71.14	1.19	20.09	3.04	0.014	1.19	0.16	ND	11.14	0.20	7.88	787.50	17.40	3.66	54.19	11.49	2.77	538.05
112215-B2	67.77	1.03	16.40	1.97	0.002	0.73	0.17	2.18	8.87	0.20	1.87	1008.93	16.30	3.74	102.81	12.82	3.44	656.48
112215-C1	98.38	0.23	1.98	0.16	ND	0.11	0.16	ND	1.55	0.17	ND	198.55	12.67	2.83	11.76	2.52	0.79	402.77
12215-C2	97.33	0.25	1.74	0.16	0.005	0.11	0.16	ND	1.49	0.15	ND	182.41	10.25	1.58	11.09	2.22	0.81	401.13
112215-D	98.10	0.25	1.56	0.26	0.003	0.09	0.16	ND	1.13	0.16	ND	151.27	9.39	1.84	11.45	2.33	0.86	431.28
MK3	93.48	0.48	5.44	0.50	0.006	0.18	0.17	ND	0.64	0.23	0.16	104.10	10.50	8.33	15.36	5.40	2.07	1006.27
MK5B	90.25	1.18	9.31	0.17	ND	0.18	0.16	ND	0.54	0.24	0.01	50.88	8.27	8.02	6.79	8.79	2.52	1231.13
MK6A	84.06	1.09	12.44	1.20	0.012	0.48	0.18	ND	1.65	0.22	0.46	199.78	10.27	6.77	26.65	11.35	3.65	1326.89
MK6	68.65	1.33	25.73	0.77	ND	0.87	0.16	ND	2.61	0.14	0.23	96.08	9.71	4.35	6.11	13.33	3.14	1091.33

Table III. Average abundances of selected trace elements. The carbonate and sandstone standards indicate average crustal abundances of elements in those rock types (Faure 1998).

	Zr (ppm)	Ba (ppm)	Th (ppm)	U (ppm)	U:Th
Carbonate Standard	19.00	10.00	1.70	2.20	1.29
Cdu Average	490.01	575.70	6.89	1.88	0.30
Sandstone Standard	220.00	10.00	1.70	0.45	0.26
Cm Average	650.78	524.97	7.59	2.08	0.30

There is a moderate positive correlation between P_2O_5 and U (R^2= 0.18) suggesting that phosphorite is not a significant source of U (Figure 12.). There is a moderate positive correlation between Zr and U in bedrock samples (R^2=0.40) (Figure 13). There is also a moderate positive correlation between Zr and Th (Figure 14). However, there are strong positive correlations between Zr and U and Zr and Th within the Dunham Dolostone samples (Figures 15 and 16). There is a moderate positive correlation between U and Th in dolostone bedrock samples (Figure 17). Lanthanum and Cerium are both present in concentrations above the average crustal abundances for carbonates (1 and 11.5 ppm respectively) (Faure 1998). La and Ce both have positive correlations with U (Figures 18 and 19). Hydrochemical data shows 1 well in the Cheshire Quartzite Formation with elevated levels of lead; geochemical data shows elevated levels of Pb in the kaolin samples from Cheshire Quartzite formation (8.02 ppm) (Appendix III), which is above the average crustal, lead chemical composition for quartzites (7.0 ppb) (Faure 1998).

A full listing of geochemical data is available in Appendix III.

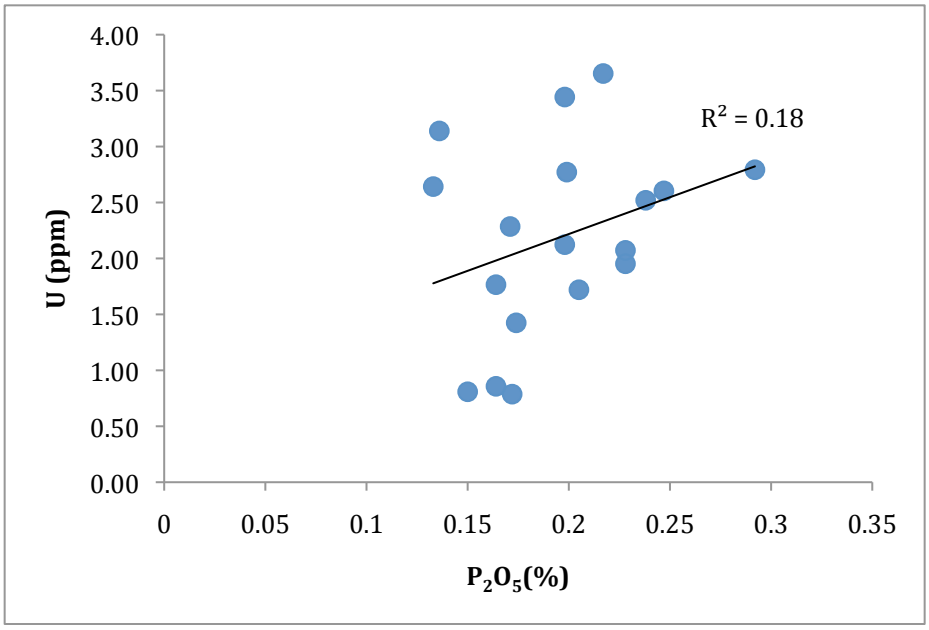

Figure 12. Moderate positive correlation between P_2O_5 concentrations and U concentrations in bedrock samples from Monkton.

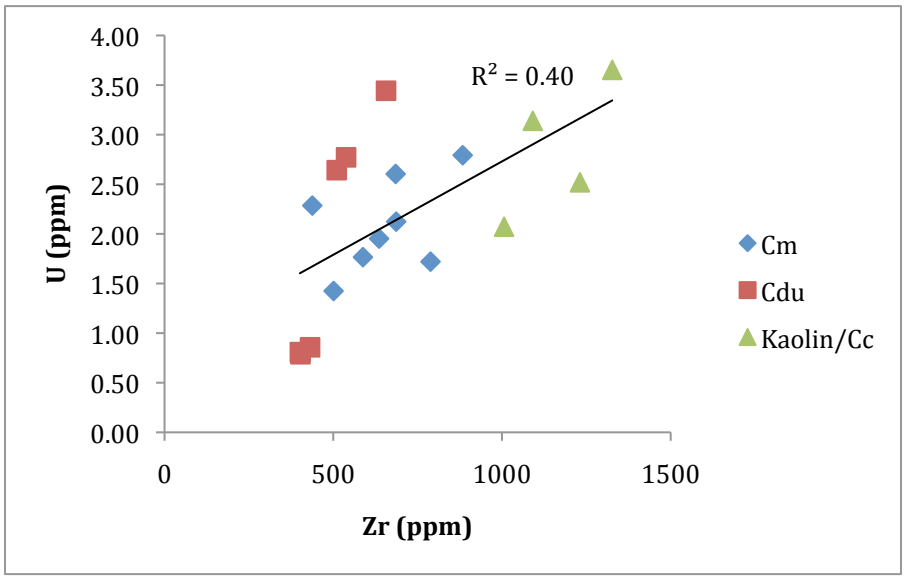

Figure 13. Moderate positive correlation between Zr concentrations and U concentrations in bedrock samples from Monkton.

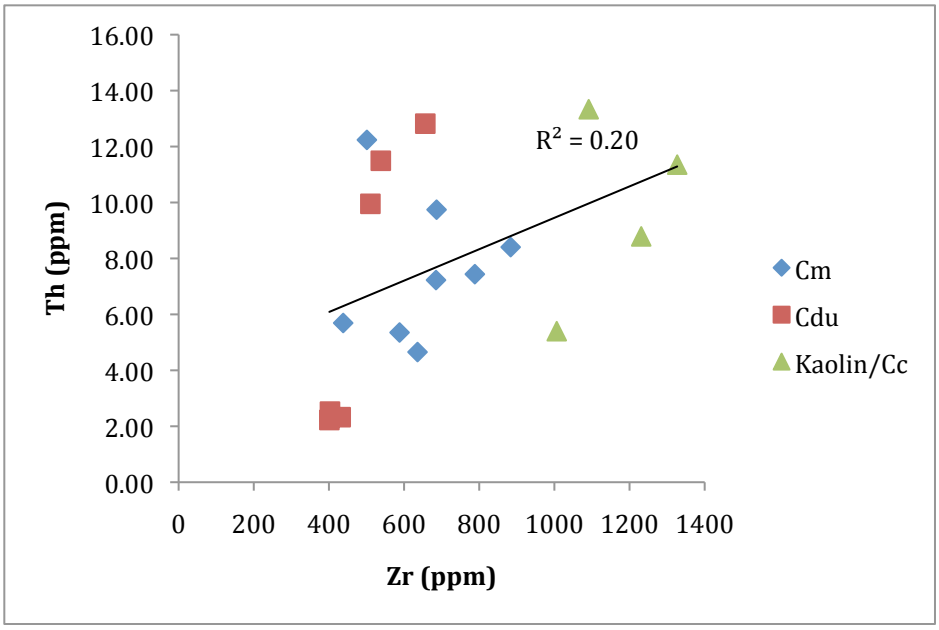

Figure 14. Moderate positive correlation between Zr concentrations and Th concentrations in dolostone samples from Monkton.

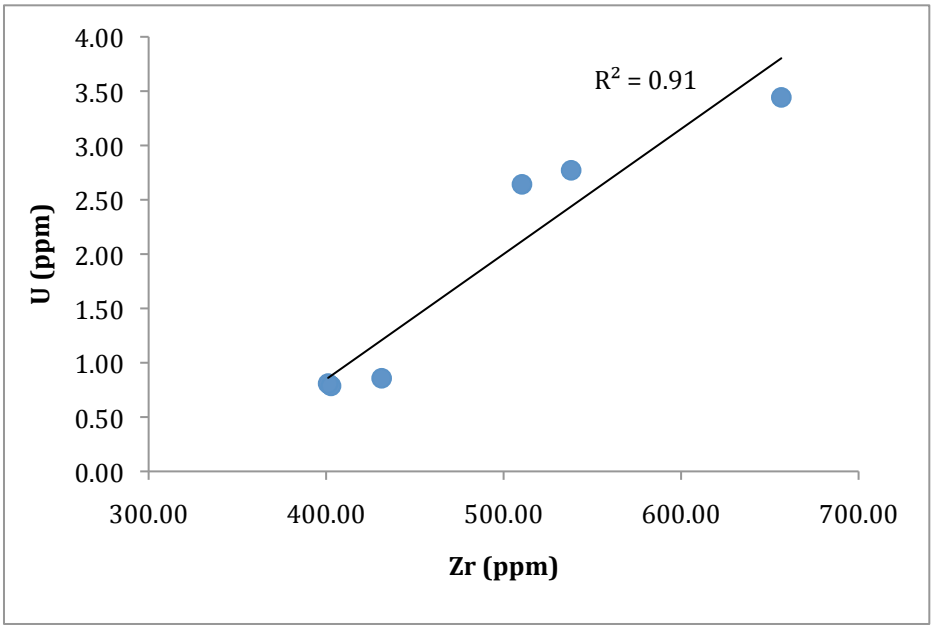

Figure 15. Strong positive correlation between Zr and U in Dunham Dolostone samples.

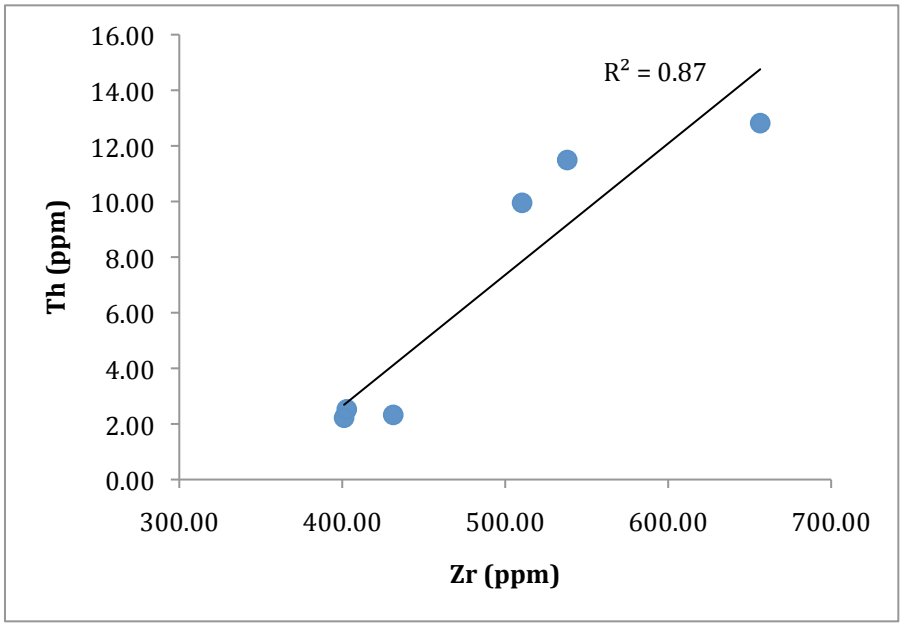

Figure 16. Strong positive correlation between Zr and Th in Dunham Dolostone samples.

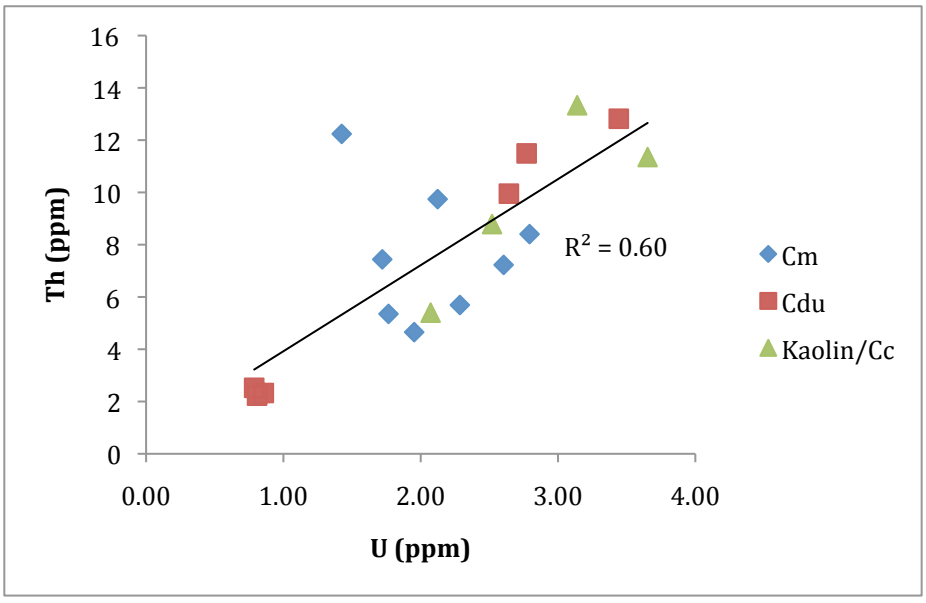

Figure 17. Positive correlation between U concentrations and Th concentrations in dolostone samples from Monkton.

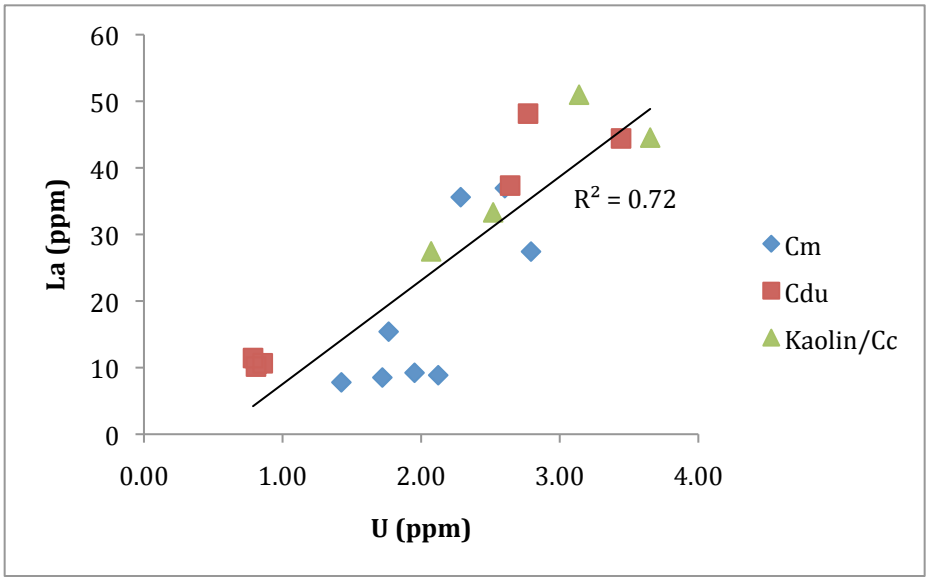

Figure 18. Positive correlation between U concentration and La concentrations in dolostone samples from Monkton.

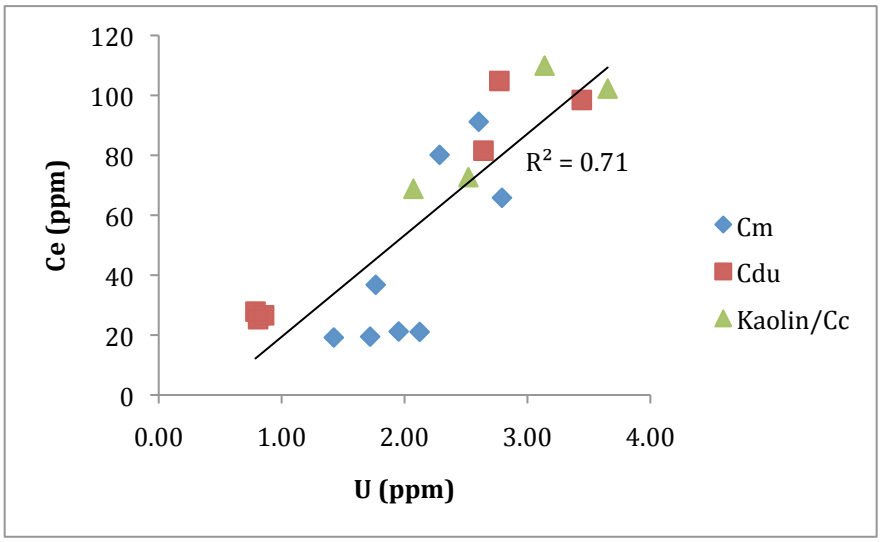

Figure 19. Positive correlation between U concentration and Ce concentrations in bedrock samples from Monkton.

IV. Well Yields

Box and whisker plots were used to compare well yields in wells producing from quartzite and dolostone bedrock wells (Figure 20). Well yields are comparable in the quartzite and dolostone bedrock wells in Monkton, as quartzite and dolostone bedrock wells produce similar medians and ranges in yield. In addition, a Mann-Whitney U statistical test shows there is no statistically significant difference in well yield in quartzite versus dolostone bedrock wells (p=0.45) (Table IV). Mean, median, range and standard deviation on well yields from data that were available of all wells in Monkton were compiled in Table V.

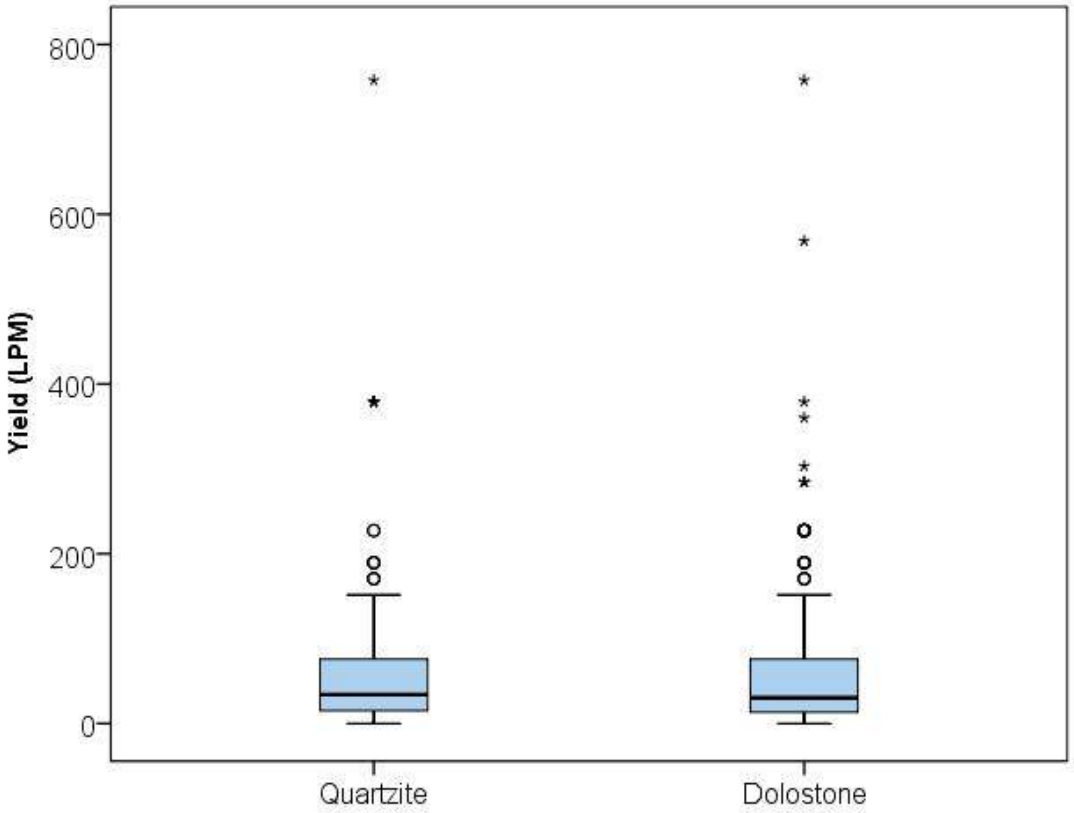

Figure 20. Box and whisker plot of all well yields in Monkton. The black line denotes the median yield. The blue box outlines the 25-75th percentile for well yield. The whiskers show the range of the 95th percentile for well yield. The open circles show outliers and stars denote extreme outliers.

Table IV. Results of a Mann-Whitney U test show there is not a statistically significant difference between quartzite and dolostone bedrock well yields in Monkton.

Mann-Whitney U	14389.0
Wilcoxon W	42830.0
Z	-0.755
Asymp. Sig. (2-tailed)	0.450

Table V. Average well yield and depth from data collected from the Well Completion Report Searchable Database *provided by the Vermont Department of Environmental Conservation grouped by bedrock type. Mean, median, range and standard deviation are in liters/minute. Yield was measured at the time the well was drilled, and may have changed since.*

	Quartzite	**Dolostone**
Mean	71.9	63.7
Median	34.1	30.2
Range	3.8-189.5	0-284.3
Standard Deviation	103.5	90.4
Number of Wells	127	238

DISCUSSION

Geochemical and hydrochemical data suggest the Dunham Dolostone and Winooski Dolostone Formations are the primary source of radionuclides in the groundwater in Monkton. Results indicate the Monkton Quartzite Formation contributes less radionuclides to groundwater than the Dunham and Winooski Dolostone Formations and older Cheshire and Pinnacle Formations in the hanging wall of the Hinesburg Thrust Fault. The original hypothesis for this study expected elevated levels of gross alpha radiation to occur in wells located in the Monkton Quartzite Formation, and lower radionuclide levels to occur in the Dunham Dolostone and Winooski Dolostone wells; data from this study suggest the opposite of this original hypothesis occurs in Monkton. The original hypothesis also originally expected, as Kim et al. (2014) suggests, lower radionuclide levels occur in the footwall of the Hinesburg thrust fault compared to the hanging wall; data from this study further suggests lower radionuclide concentration occur in the footwall compared to the hanging wall. Suggestions for radionuclide concentrations are explored. Suggestions for elevated levels of lead in Cheshire Quartzite are elevated levels of manganese in the Monkton Quartzite are also explored.

I. Elevated levels of Gross Alpha Radiation: Mineralogical Origins

Zircon

Elevated levels of gross alpha radiation were found in the Dunham Dolostone and Winooski Dolostone Formations; elevated levels of gross alpha radiation, however, are an order of magnitude lower than gross alpha radiation in the hanging wall (dominantly siliciclastic), where Kim et al. (2014) found average gross alpha to be 18.3 pCi/L with a

range of 1.1-107 pCi/L (N=25). Dunham Dolostone and Winooski Dolostone samples in the footwall had an average gross alpha value of 4.9 pCi/l and a range of <1.5-12.9 pCi/L (N=9). This is higher than the Monkton Quartzite average alpha value of 2.8 pCi/l and a range of <1.5-4.28 pCi/L (N=14). Similarly, a study by Kim and Thompson (2002) found no elevated levels of gross alpha radiation in wells in the Monkton Quartzite. Bean (2009), however, found some wells drawing from the Monkton Quartzite with elevated gross alpha radiation (3 out of 6 wells; average of 5.7 pCi/l).

The strong positive correlation between gross alpha and U indicate elevated levels of radionuclides in the Dunham Dolostone and Winooski Dolostone Formations in the groundwater are a product of U-decay. North concludes that U is the ultimate source of elevated gross alpha radiation in the Cheshire, Fairfield Pond, and Pinnacle Formations in the hanging wall (North 2005). Kim et al. (2014) also suggests a correlation between elevated levels of U and gross alpha radiation. Dissimilarly, Bean found essentially no correlation between U and Ba in the footwall of the Hinesburg thrust fault, and suggested U resides in additional minerals. Bean (2009) suggests that U is derived from younger carbonated dominated units in the footwall in calcite and phosphate minerals (such as apatite).

The positive correlation between Zr and U (R^2=0.4) suggests these radioactive isotopes might be substituting into the zircon crystal lattice. The Dunham Dolostone Formation exhibits strong positive correlations between Zr and U (R^2=0.91) and Zr and Th (R^2=0.87), supporting that zircon crystals are a probable source of elevated gross alpha radiation. The rare earth elements cerium and lanthanum are common in monazite, zircon and apatite. The positive correlation between cerium and U and lanthanum and U

further suggest the presence of radioactive-bearing minerals (Deer et al. 1966). North (2005) also found a strong positive correlation between Zr and U, further suggesting zircon as a source of gross alpha radiation in the hanging wall. The positive correlation between U and Th (R^2=0.60) suggests both might be derived from the same mineral source and might both be responsible for elevated levels of radionuclides in the dolostone bedrock aquifer. North similarly found a strong correlation between Th and U (R^2=0.89), and North (2005) and Bean (2009) similarly found strong positive correlations between Th and Zr, indicating zircon as a potential source of gross alpha radiation.

Detrital materials typically have U:Th ratios ranging from 0.25-0.33 (Peter Ryan, personal communication). The average U:Th ratio for the Dunham Dolostone (0.30) and Monkton Quartzite (0.30) imply U is sourced by a detrital mineral. U:Th ratios suggests that continental erosion transport into the shallow marine depositional environment of the Monkton Quartzite and Dunham Dolostone resulted in the deposition of zircon containing U and Th in the footwall of the Hinesburg Thrust Fault. Kim et al. (2014) similarly suggest that zircons included in the fault zone in metamorphosed rocks of the hanging wall and footwall have detrital origins, but also suggests metamorphic origin for zircons in the hanging wall and fault zone as an additional possibility. North (2005) similarly suggests detrital source for zircons enriched in Th. Bean (2009), however, suggests that U co-precipitated out of seawater into limestones in carbonate units in the footwall of the Hinesburg Thrust Fault, noting U:Th ratio >1 (high U, low Th).

Elevated (but comparable) levels of Zr occur in different formations throughout the Champlain Valley Sequence compared to average crustal abundances (Table VI). Perhaps radionuclide levels in groundwater are not dependant on abundance of Zr, but

perhaps availability of U and Th within the crystal structure. Trace minerals such as zircon are often resistant to breakdown in groundwater (Balan et al. 2001). However, zircon and other radionuclide bearing minerals are made more susceptible to breakdown and release of U, Th and decay products in groundwater though internal radiation damage (Woodhead et al. 1991, Kim et al. 2014) and grain size reduction and dissolution in shear zones (Dempster et al. 2008, Kim et al. 2014). There is evidence of fractured and cleaved zircons along disjunctive cleavage planes in the phyllitic quartzites of the Cheshire and Pinnacle Formation (North 2005, Kim et al. 2014), compared to relatively intact zircons in the Monkton Quartzite (Figures 21a-21c.). It is possible these zircons either have metamorphic origins or (as suggested by U:Th ratios) were detrital zircons and were enveloped by the cleavage plane (Kim et al. 2014). The location of these zircons within a cleavage plane would allow contact with groundwater flow. These zircons are a possible source of radionuclides in the Cheshire and Pinnacle Quartzite. Bedrock samples collected from the Dunham Dolostone formation displayed shearing and deformation. It is possible that deformation decreased the surface area through fracturing and cleaving of the zircons and made U more available in the dolostone in the footwall. Conversely, the Monkton Quartzite remains relatively undeformed. It is fractured, but not cleaved like the Pinnacle Formation in hanging wall of the Hinesburg Thrust Fault. Relatively intact zircon in the Monkton quartzite have less surface area and provide less opportunity to release available U and Th into the groundwater aquifer.

Table VI. Average Zr concentration in different bedrock formations and average crustal abundances. Average crustal abundances (*) provided by Faure, 1998. Average Cheshire Quartzite, Fairfield Pond, and Pinnacle Quartzite abundances (**) provided by Kim et al. 2014.

	Average Zr
Carbonate Crustal Average*	19 ppm
Sandstone Crustal Average*	220 ppm
Monkton Quartzite	651 +/- 145 ppm
Dunham Dolostone	490 +/- 99 ppm
Cheshire Quartzite**	577 +/- 248 ppm
Fairfield Pond**	411 +/- 158 ppm
Pinnacle Quartzite**	541 +/- 280 ppm

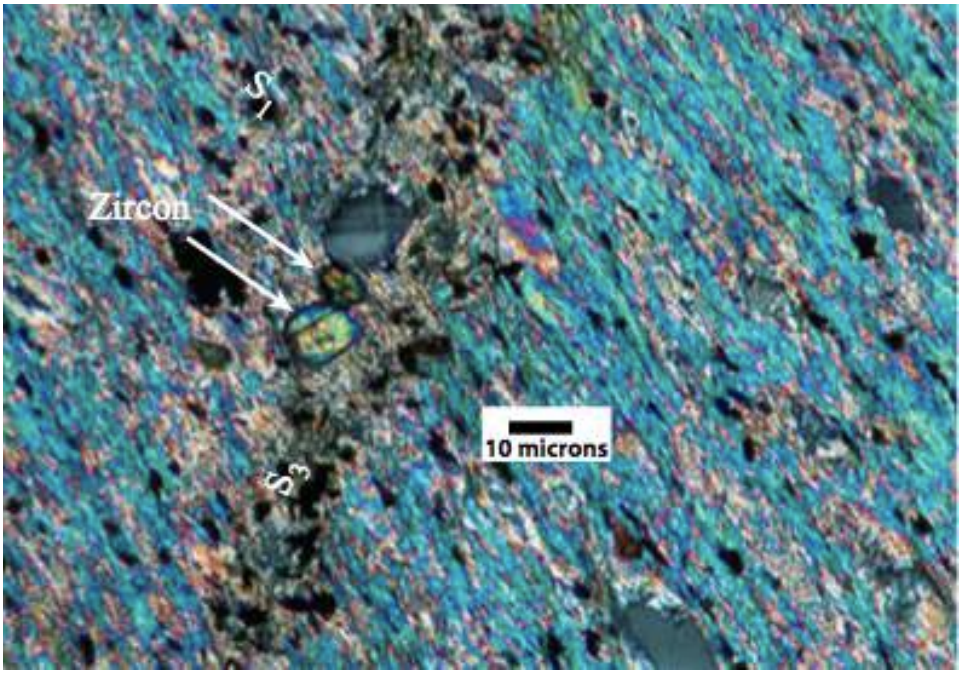

Figure 21a. Zircon grains along a cleavage plane from the Cheshire Quartzite formation in the hanging wall of the Hinesburg thrust (crossed polarized light). The zircons are not euhedral in shape, and contain evidence of fractures (Kim et al. 2014).

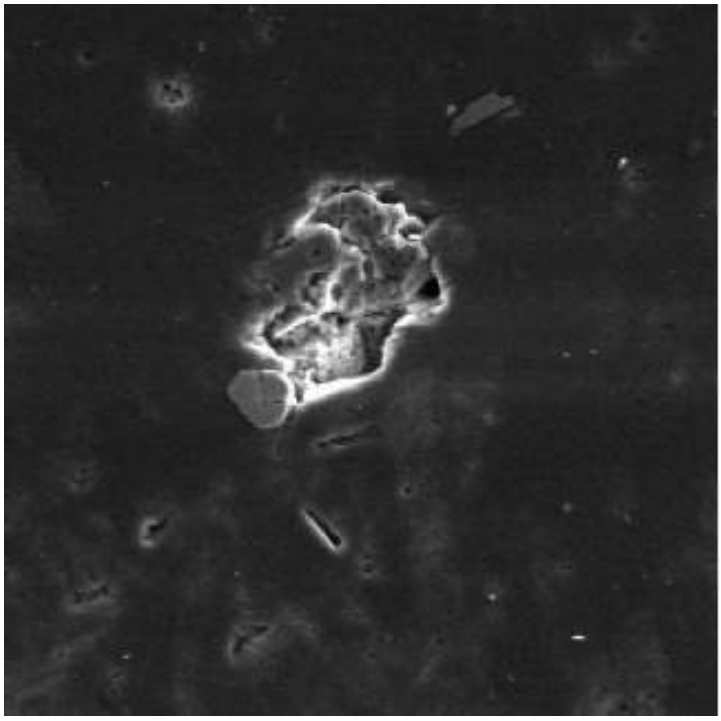

Figure 21b. Fractured and cleaved grains of zircon and apatite in the Pinnacle Formation in the hanging wall of the Hinesburg Thrust fault. This photograph is taken in BSE mode and is approximately 50 microns wide (North 2005).

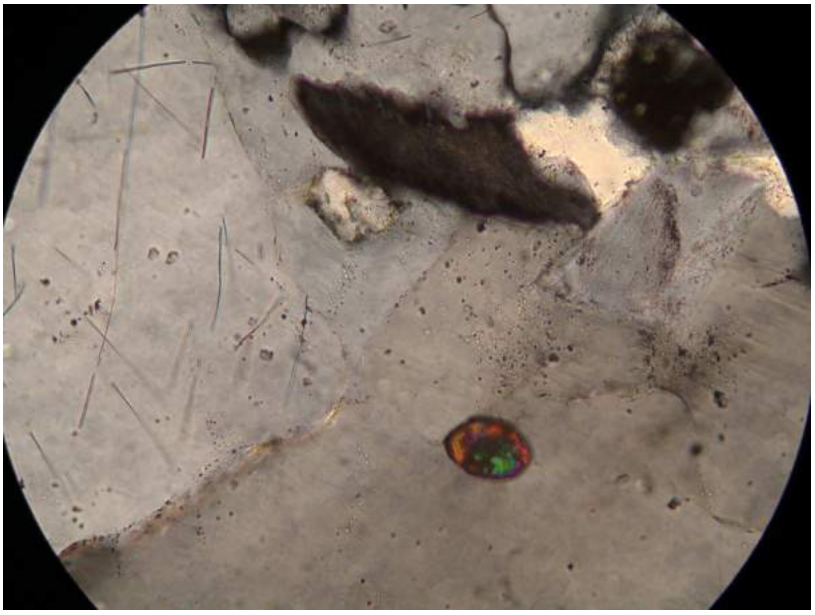

Figure 21c. Euhedral zircon in Monkton Quartzite (40x). Photograph provided by Charlotte Mehrtens

Compositional Differences

Differences in radionuclide levels in the Hinesburg thrust fault hanging wall quartzites and footwall quartzites might be a product of differences is rock geochemistry. The hanging wall of the Hinesburg thrust fault is dominated by the Cheshire, Fairfield Pond, and Pinnacle phyllitic quartzite Formations. The Pinnacle, Fairfield Pond and the Cheshire Formations are comprised of sediments deposited during the late Proterezoic to early Cambrian early rift and drift stages of the Iaptus Ocean. Monkton quartzite, present in the footwall of the Hinesburg thrust fault, is composed of sediment deposited on the passive Laurentian continental margin as spreading of the Iaptus Ocean continued from the early Cambrian to the Middle Ordovician (Kim et al. 2014). Difference in older sediments deposited during the early rift and drift stages versus the younger sediments deposited in the passive margin could account for compositional differences between the hanging wall and footwall quartzites. In addition, U and Th concentrations are slightly lower in the Monkton Quartzite (U mean= 2.08 ppm, Th =7.59 ppm) relative to the Cheshire and Pinnacle Formation (U mean= 2.6 ppm, Th mean=12.6 ppm), and might contribute to differences in elevated radionuclide levels in the hanging wall versus footwall.

II. Difference in water reactions

Ca-Mg Bicarbonate Signature

Chemical classification using a piper diagram show the groundwater has a dominantly Ca-Mg bicarbonate signature. This indicates the dissolution of carbonate has a large impact on groundwater chemistry. This is likely due to the presence of dolostone

in the bedrock formations. Carbonates are very soluble, so small amounts of carbonates allow carbonate signatures to dominate the groundwater chemistry (Langmuir 1997). Carbonates have a buffering capacity, and yield neutral pH. It is possible the carbonate dominated groundwater signature leads to neutral groundwater, which would lower solubility.

Co-precipitation of barite

Differences in radionuclide levels in the quartzite aquifers of the Hinesburg hanging wall and footwall could be due to hydrochemical reactions. One possibility is that radium is sequestered through the co-precipitation of barite. A study by Senior and Vogel (1995) on the Cambrian Chickies Quartzite Formation in Southeastern Pennsylvania shows that radionuclide levels are indirectly related to barium concentration due to the sequestration of Ra.

Groundwater samples from Monkton contained high levels of Ba compared to average Ba concentration in the hanging wall and footwall (footwall average= 41.6 ppb, hanging wall average= 95.0 ppb, Monkton average= 106.3 ppb) (Table VIIa). It is possible this elevated level of Ba in the groundwater leads to the precipitation of barite. Geochemical data shows Ba is abundant throughout the region. Monkton quartzite bedrock samples from Monkton have higher concentrations of Ba compared to the average footwall concentration (Cm average= 525.0 ppm, footwall average= 118.0 ppm). Dunham Dolostone bedrock samples also have high concentrations of Ba compared to the average footwall (Cdu average= 576.7 ppm) (Table VIIb, Appendix III.). This suggests in Ba in the bedrock contributes to elevated levels of Ba in the groundwater. Elevated

levels of Ba are likely due to the abundance of quartzite and slate beds in the Dunham Dolostone and Monkton Quartzite formations. XRD data indicates the presence of feldspars in Monkton quartzite samples collected in Monkton, which has the potential to hold Ba. The precipitation of barite in the footwall could be a method of Ra sequestration, and could contribute to relatively low levels of gross alpha radiation observed in the footwall of the Hinesburg Thrust fault relative to the hanging wall, as well as low radionuclide levels in the Monkton Quartzite Formation.

Table VIIa. Average, standard deviation and range of Ba in groundwater. Data for the footwall and hanging wall from Kim et al. (2014).

	Mean (ppb)	SD (ppb)	Min (ppb)	Max (ppb)
Footwall	41.6	34.9	<5	147
Hanging wall	95.0	51.5	33.9	171.0
Samples from Monkton, VT	106.3	106.7	5.0	397.5

Table VIIb. Whole rock average, standard deviation, and range of Ba. Data for the footwall and hanging wall from Kim et al. (2014).

	Mean (ppm)	SD (ppm)	Min (ppm)	Max (ppm)
Footwall	118.0	148.0	13	533
Hanging wall	858	383	50	1587
Monkton Quartzite	525.0	319.8	94.0	1021.3
Dunham Dolostone	575.7	449.9	151.3	1125.6

III. Physical hydrology

It is unlikely residence time contributes to differences in radionuclide levels in Monkton. Wells that produce from quartzite and dolostone bedrock generate similar mean, median and range in yields. In addition, the difference in yield in wells in the

quartzite and dolostone bedrock aquifers were not statistically significant (p=0.45).

Bean's (2009) study of the bedrock aquifer wells in Hinesburg, VT, (north of Monkton) included well samples from the footwall of the Hinesburg thrust fault. This study included six Monkton Quartzite bedrock well samples. Of these six, three water samples contained elevated levels of gross alpha radiation. In his study, the average yield of Monkton Quartzite bedrock wells was 74.5 l/min, and average depth was 97.2 m. Similar yield results in average yield of Monkton Quartzite bedrock wells in Monkton compared to Bean's (2009) study section in the footwall further suggest yield does not account for concentration of alpha radiation in the footwall.

Residence times might contribute to the order of magnitude of difference in radionuclides levels between the hanging wall and footwall. Kim et al. (2014) suggests the median well yield is lower in the hanging wall of the Hinesburg thrust fault compared to the footwall. The average well yield for quartzite and dolomite wells in Monkton is also notably higher than the average Hinesburg hanging wall yield (Table VIII.). This could be a product of dolomitic layers within the Monkton Quartzite, which enhances solubility, and therefore enhances groundwater flow. The quartzites in the hanging wall, unlike the Monkton Quartzite, do not contain dolomitic layers (Peter Ryan, Personal Communication).

Table VIII. Average well yield and depth data from wells tested in this study compared to average well yield and depth data published in Kim et al. 2014.

	Cm	Cdu	Hinesburg Footwall (Kim et al. 2014)	Hinesburg Hanging Wall (Kim et al. 2014)
Average Yield (lpm)	71.9	63.7	53.5	5.0
Number of Wells	127	238	34	22

As previously mentioned, Zircon is a likely source for elevated radionuclides in the hanging wall of the Hinesburg thrust fault (Kim et al. 2014). Higher levels of Zr occur in the Monkton Quartzite relative to the Hinesburg Thrust Fault, but it is possible this zircon is relatively unavailable (Appendix III). Perhaps a combination of high yield in the Monkton Quartzite and relatively unavailable zircon lend to lower gross alpha radiation in the Monkton Quartzite aquifer.

IV. Elevated Level of Lead

One well in the Cheshire Quartzite Formation contained elevated levels of lead (22.5 ppb). It is located near the St. George Thrust Fault. It is possible that hydrothermal fluids that altered the Cheshire Quartzite Formation (Stanley 1980, Nichols 2001) may be responsible. Hydrothermal fluids flowed along the Mesozoic St. George fault and altered the Cheshire Quartzite (Ogden 1969), so it is possible that these hydrothermal fluids carried in lead from older formations (such as the Mendon Formation) or from a different origin.

V. Elevated Levels of Manganese

Elevated levels of manganese were found in 2/28 wells, both of which were in the Monkton Quartzite. In addition, one well studied by Bean (2009), also in the Monkton Quartzite, had elevated levels of manganese (378 µg/L). Data from Kim et al. suggest manganese concentrations are higher in the footwall compared to the hanging wall of the Hinesburg thrust fault (Table IX). Dolomite is normally close to pure $CaMg(CO_3)_2$, however, Mn can replace Mg (Deer et al. 1966). It is possible Mn replaced Mg in

dolomitic layers within the Monkton Quartzite. Mn also occurs in iron oxides and hydroxides, so reducing conditions deeper in the aquifer might cause the release of Mn to solution (Ryan et al. 2013).

Table IX. Average, standard deviation and range of Mn in bedrock from the footwall and hanging wall of the Hinesburg Thrust fault. Data from the footwall and hanging wall from Kim et al. (2014).

	Mean (ppm)	**SD (ppm)**	**Min (pp)**	**Max (ppm)**
Footwall	43.7	91.7	<5	378
Hanging wall	14.3	2.4	11.2	20.3
Cm	77.0	180.8	<5	563.0

CONCLUSION

The bedrock aquifer in Monkton, Vermont had appreciably lower concentrations of gross alpha radiation than the bedrock aquifer in the hanging wall of the Hinesburg Thrust Fault (Kim et al. 2014), and similar values to the footwall (Bean 2009). While gross alpha radiation is low relative to the Hinesburg Thrust Fault hanging wall, locally elevated gross alpha radiation in Monkton in the Dunham Dolostone and Winooski Dolostone could be from U in fractured and cleaved zircon crystals. A combination of high well yields and a lower degree of deformation of the Monkton Quartzite lends to lower radionuclide levels in the Monkton Quartzite bedrock aquifer. It is also possible the co-precipitation of Ra and barite lead to lower radionuclide levels in the footwall. It is possible elevated levels of manganese are due to Mn replacement of Mg in dolomitic beds, or due to release of Mn into solution reducing conditions deeper in the bedrock. Elevated levels of lead in the Cheshire Quartzite might be a product of hydrothermal fluids that flowed through the formation along the St. George Thrust Fault.

This study can be a useful model for groundwater studies in Vermont, as well as other locations with similar bedrock units. Controls on bedrock aquifer quality remain poorly understood in the scientific community. In addition, sandstone and quartzite are common aquifer materials that often (but not always) have high radionuclides.

Future research should include the geochemical analyses of bedrock closer to the sources of elevated radionuclides. It is possible that variation in the bedrock lithology leads to variety of concentration of naturally occurring inorganic constituents in the bedrock aquifer. Future research should also examine other quartzite and carbonate

bedrock aquifers in the Champlain Valley, as the wide range in aquifer potential observed in the regional bedrock aquifer in the region is not yet fully understood.

Appendix I: Bedrock Sampling Sites and Lithology

	Lat	Long	Fm	Lithology
082815-1A	44.2192	-73.1537	Cm	Reddish-silty quartzite with Fe-hx on fractures
082815-1B	44.2192	-73.1537	Cm	Coarse-grained purple quartzite interbedded with medium-grained white quartzite
082815-1C	44.2192	-73.1537	Cm	Pink and purple quartzite, dolomitic cement, well defined bedding plane, brown weathering
082815-1D	44.2192	-73.1537	Cm	Weathered rusty-tan dolomitic sandstone, friable, located on top of outcrop
082815-2A	44.2413	-73.1559	Cm	Interbedded fine-grained purple quartzite and green mudstone, slickens form chlorite
082815-2B	44.2413	-73.1559	Cm	Pink and green coarse-grained quartzite, brown weathering, some pebbles
082815-3A	44.2416	-73.1562	Cm	Fine-grained, sandy greenish-grey mudstone
082815-3B	44.2416	-73.1562	Cm	Reddish-brown dolomitic sandstone, weathered
112215-A	44.2177	-73.1156	Cdh	Red-brown quartzite with thin slate layers
112215-B1	44.2177	-73.1156	Cdh	Sheared metasedimentary rock with shale component
112215-B2	44.2177	-73.1156	Cdh	Shaley, phyllitic metasedimentary rock
112215-C1	44.2257	-73.1169	Cdh	Greenish gray medium-grained quartzite
112215-C2	44.2257	-73.1169	Cdh	Reddish-pink quartzite
112215-D	44.2257	-73.1169	Cdh	Dark reddish-brown quartzite
MK3	44.1667	-73.0833	Cc	White, sandy clay
MK5B	44.1667	-73.0833	Cc	Weathered quartzite rock bottom
MK6	44.1667	-73.0833	Cc	Very fine-grained white clay
MK6A	44.1667	-73.0833	Cc	1-2cm thick gray clay layer within massive white clay

Appendix II: Hydrochemical Data

Sample ID	Bedrock Type	Gross Alpha (pci/liter)	Alkalinity (mg CaCO3/L)	Aluminum (ug/L)	Antimony (ug/L)	Arsenic (ug/l)	Barium (ug/L)	Beryllium(ug/L)	Cadmium (ug/L)	Calcium (ug/L)	Chloride (ug/L)	Chromium (ug/L)	Cobalt (ug/L)
083115-1	Cm	<1.5	198	<50	<10	<1	172.1	<1	<1	42.88	0.86	<5	<1
090115-1	Cm	3.2	256	<50	<10	<1	46.67	<1	<1	41.71	4.354	<5	<1
090115-2	Cm	3.35	196	<50	<10	<1	32.83	<1	<1	62.44	1.04	<5	<1
090115-3	Cm	2.15	276	<50	<10	<1	78.48	<1	<1	47.69	9.026	<5	1.588
090815-1	Cdu	12.9	238.5	<50	<10	<1	24.02	<1	<1	58.12	1.21	<5	<1
090815-2	Cdu	1.52	129	<50	<10	<1	36.05	<1	<1	43.46	0.27	<5	<1
90915-1	Cm	2.3	157	<50	<10	2.545	161.5	<1	<1	20.19	1.25	<5	<1
90915-2	Cdu	2.15	300	<50	<10	<1	217.9	<1	<1	72.74	2.5	<5	<1
091115-1	Cm	3.27	215	<50	<10	<1	246.7	<1	<1	39.9	1.05	<5	<1
091115-2	Cm	2.97	176	<50	<10	<1	98.47	<1	<1	34.09	0.64	<5	<1
091715-1	Cdu	2.71	220	<50	<10	<1	21.71	<1	<1	54.8	1.33	<5	<1
091715-2	Cm	<1.5	271	<50	<10	<1	13.29	<1	<1	74.03	20.31	<5	<1
091715-3	Cm	<1.5	227	<50	<10	<1	187.6	<1	<1	55.44	0.92	<5	<1
091715-4	Cm	3.09	393	<50	<10	<1	397.5	<1	<1	113.5	14.2	<5	<1
092415-1	Cw	7.38	245	<50	<10	<1	187.9	<1	<1	47.46	8.617	<5	<1
092415-2	Cm	4.06	228.5	<50	<10	<1	286	<1	<1	34.91	6.373	<5	<1
093015-1	Cc	<1.5	106	<50	<10	<1	5.821	<1	<1	29.21	0.43	<5	<1
093015-2	Cc	2.75	30	<50	<10	<1	6.945	<1	<1	11.32	3.12	<5	<1
100115-1	Cm	3.73	211	<50	<10	<1	142.8	<1	<1	29.9	0.39	<5	<1
101515-1	Cm	4.28	218	<50	<10	<1	258.2	<1	<1	29.08	0.56	<5	<1
101515-2	Cc	>1.5	27	<50	<10	<1	18.81	<1	<1	10.38	2.17	<5	<1
101515-3	Cdu	<1.5	35	<50	<10	<1	5.691	<1	<1	8.309	0.28	<5	<1
101515-4	Cdu	10.3	248	<50	<10	<1	19.39	<1	<1	58.58	1.96	<5	<1
101615-1	Cc	<1.5	22	<50	<10	<1	5.042	<1	<1	4.622	0.42	<5	<1
102215-1	Cdu	2.53	211	<50	<10	<1	35.95	<1	<1	50.35	1.88	<5	<1
102315-1	Cm	2.03	228	<50	<10	<1	187.3	<1	<1	42.56	0.84	<5	<1
121615-1	Cdu	2.87	70	<50	<10	<1	45.16	<1	<1	19.96	2	<5	<1
121615-2	Cm	1.88	222	<50	<10	<1	37.54	<1	<1	40.82	2.04	<5	1

Sample ID	Bedrock Type	Copper (ug/L)	Fluoride (ug/L)	Iron (ug/L)	Lead (ug/L)	Magnesium (ug/L)	Manganese (ug/L)	Mercury (ug/l)	Molybdenum (ug/L)	Nickel (ug/L)	Nitrate (mg N/l)
083115-1	Cm	10.82	<0.5	50	<1	39.77	<5	<0.2	<5	<5	0.02
090115-1	Cm	<10	<0.5	134.7	<1	26.65	<5	<0.2	<5	<5	1.19
090115-2	Cm	<10	<0.5	119.9	<1	38.73	<5	<0.2	<5	<5	0.2
090115-3	Cm	10.47	<0.5	50	<1	22.11	475.7	<0.2	<5	<5	0.51
090815-1	Cdu	<10	<0.5	109.8	<1	32.97	131.2	<0.2	<5	<5	0.02
090815-2	Cdu	<10	<0.5	405.4	<1	9.926	156.5	<0.2	<5	<5	0.02
90915-1	Cm	13.91	<0.5	50	<1	15.12	<5	<0.2	<5	<5	0.02
90915-2	Cdu	<10	<0.5	151.1	5.788	37.71	18.75	<0.2	<5	<5	0.13
091115-1	Cm	<10	<0.5	50	3.07	32.94	<5	<0.2	<5	<5	0.07
091115-2	Cm	<10	<0.5	64.01	<1	21.7	<5	<0.2	<5	<5	0.26
091715-1	Cdu	<10	<0.5	72.06	<1	30.21	<5	<0.2	<5	<5	0.51
091715-2	Cm	<10	<0.5	50	<1	37.51	<5	<0.2	<5	<5	0.8
091715-3	Cm	10.16	<0.5	50	<1	29.49	<5	<0.2	<5	<5	0.07
091715-4	Cm	34.91	<0.5	50	12.59	61.75	563	<0.2	<5	<5	0.38
092415-1	Cw	<10	<0.5	50	<1	40.57	<5	<0.2	<5	<5	1.23
092415-2	Cm	<10	<0.5	50	<1	36.08	56.74	<0.2	<5	<5	0.02
093015-1	Cc	<10	<0.5	50	<1	11.74	<5	<0.2	<5	<5	0.12
093015-2	Cc	321.1	<0.5	187.5	22.1	3.57	9.668	<0.2	<5	<5	0.62
100115-1	Cm	<10	<0.5	139.1	<1	38.13	<5	<0.2	5.042	<5	0.02
101515-1	Cm	<10	<0.5	50	<1	37.68	<5	<0.2	<5	<5	0.07
101515-2	Cc	83.96	<0.5	562.9	7.138	3.231	8.533	<0.2	<5	<5	1.29
101515-3	Cdu	36.43	<0.5	50	<1	3.034	<5	<0.2	<5	<5	0.39
101515-4	Cdu	14.75	<0.5	83.68	<1	32.19	<5	<0.2	6.777	<5	0.07
101615-1	Cc	25.15	<0.5	241.7	<1	2.239	28.88	<0.2	<5	<5	0.02
102215-1	Cdu	<10	<0.5	170	<1	27.24	<5	<0.2	<5	<5	1.03
102315-1	Cm	<10	<0.5	50	<1	31.75	<5	<0.2	<5	<5	0.15
121615-1	Cdu	<10	<0.5	50	<1	9.573	<5	<0.2	<5	<5	0.17
121615-2	Cm	<10	<0.5	97.68	<1	36.1	<5	<0.2	<5	<5	0.62

Appendix III: Geochemical Data

Whole Rock: Trace Elements

	45Sc [ppm]	51V [ppm]	52Cr [ppm]	59Co [ppm]	60Ni [ppm]	63Cu [ppm]	66Zn [ppm]	75As [ppm]	85Rb [ppm]	88Sr [ppm]	89Y [ppm]
082815-1A	6.674270909	43.13642703	20.46015517	25.76418584	16.50025521	14.61308808	78.74066971	0.670663225	122.3114572	88.91692746	51.30278939
082815-1B	2.37350872	7.865603476	4.921593163	78.3896705	16.86935028	19.53832859	530.2352741	0.438018219	9.96278734	9.266278328	14.18751827
082815-1C	5.118834411	23.16696983	10.4771167	37.30507103	46.23283731	22.5890616	555.5780021	0.501014987	50.3087398	91.87055283	34.8841756
082815-1D	5.925404793	18.37048943	8.890448959	30.64930994	18.60247814	20.84782608	519.1448605	0.779033166	28.84783869	61.21864042	34.22824038
082815-2A	6.94539421	32.59841219	13.97882639	28.47177088	16.1286947	19.63545767	587.817211	1.409300519	67.20334735	58.94281984	59.98701827
082815-2B	3.89990432	15.32826152	6.500588853	64.63942531	12.17050527	16.62042661	93.27415062	0.252897568	20.87975811	87.08030199	24.17834843
082815-3A	8.730564322	54.31224044	24.29108263	16.07173096	13.29358286	9.041214846	110.5717076	0.785869834	132.1474358	64.12162296	55.14044613
082815-3B	4.765039976	19.72986736	9.588596732	28.99152197	15.88363243	18.49345895	64.1372357	2.077850598	33.30725432	33.62698508	33.12802653
112215-A	6.893678138	45.04126077	29.41072021	60.97172697	20.99049517	14.58157192	35.89924483	7.021743979	111.9517841	86.8152188	34.17527385
112215-B1	11.31350093	79.145281	45.52676135	15.13582259	19.10524643	17.40220086	17.03295786	7.878532559	119.5689197	54.19038062	38.82086991
112215-B2	9.82101951	64.05045959	36.67740509	28.5621098	14.27424869	16.30199406	7.607601269	1.866447081	113.0911486	102.8122505	47.77071329
112215-C1	1.354427074	4.579524933	5.237012617	54.95995763	10.09950436	12.66536958	17.18636817	-0.107763559	15.03838379	11.75811408	13.49603317
12215-C2	1.311897048	4.215760105	4.975964853	93.93541606	9.553456108	10.25207971	5.128654628	-0.092269316	12.40143862	11.09480214	12.94615406
112215-D	1.724111788	6.374877459	4.561158449	46.61446563	5.453781835	9.389247613	1.2182826	-0.105628996	10.91169453	11.44966974	9.725327122
MK3	4.113886394	19.86082466	14.01725219	16.90201586	11.76620377	10.49752677	5.000912804	0.159781257	12.85748488	15.36002206	25.33392586
MK5B	6.478708275	26.53224078	17.07685623	25.68443553	9.32677284	8.272837092	-0.161981616	0.00622782	8.457647377	6.792962698	34.2600424
MK6A	9.172472202	42.72176039	27.28389123	37.96676561	11.06143826	10.27331914	2.168973341	0.4587046	31.03107493	26.64793356	48.58660707
MK6	11.16923882	65.61131496	38.40052409	1.83614639	13.08066365	9.708915369	1.892859162	0.225768749	49.45630456	6.111557943	51.28988605

	90Zr [ppm]	93Nb [ppm]	103Rh	115In	137Ba [ppm]	178Hf [ppm]	181Ta [ppm]	208Pb [ppm]
082815-1A	437.9551606	13.29655817	89.40%	90.30%	1021.283203	12.62510526	1.101842868	18.017847
082815-1B	501.0134707	6.668997953	90.40%	92.80%	93.95662453	14.23327999	1.103171802	9.100619797
082815-1C	588.0055413	10.87472013	86.50%	88.60%	470.373581	18.11830726	1.019179814	15.32555636
082815-1D	686.4896511	11.25489535	84.20%	87.70%	371.5043425	21.68293066	1.09262804	17.75055822
082815-2A	883.6491226	16.88420306	82.30%	85.10%	569.7252154	28.14697727	1.466052666	27.01669097
082815-2B	788.3725387	5.470439527	114.60%	81.00%	272.8899729	20.60201722	0.896429686	17.78231921
082815-3A	684.9594017	16.14980535	68.30%	68.80%	955.5538967	22.8562281	1.233063664	42.74741557
082815-3B	635.802869	6.920426287	80.20%	84.00%	444.4709257	18.93050716	0.538631917	16.70973863
112215-A	510.3455895	17.90051939	81.90%	83.10%	1125.552239	16.77602117	1.39462251	20.56587503
112215-B1	538.0538337	21.22408048	102.10%	87.90%	787.503557	15.49182339	1.348721932	3.656025459
112215-B2	656.4755909	21.31680934	99.90%	90.20%	1008.933478	19.73240183	1.38933655	3.740115515
112215-C1	402.7676111	4.210349969	90.00%	80.40%	198.549299	11.31022783	0.370670627	2.827751912
12215-C2	401.1328961	4.07435268	0.919	0.824	182.4061645	11.14886997	0.946097096	1.58343843
112215-D	431.2845981	3.85690296	91.20%	82.30%	151.2666698	12.15203782	0.453301691	1.83953668
MK3	1006.273026	8.370520115	91.20%	83.40%	104.0968233	29.96490963	0.564737443	8.328846915
MK5B	1231.129399	17.05402217	91.60%	83.40%	50.88404383	38.73392592	1.448980761	8.024722962
MK6A	1326.892815	19.96602078	90.10%	80.50%	199.7766172	42.23422729	1.738942157	6.766300605
MK6	1091.330398	27.63946711	88.70%	80.90%	96.08398885	35.42002558	1.883408587	4.353116448

Whole Rock: Rare Earth Elements

	45Sc [ppm]	89Y [ppm]	103Rh	133Cs	139La [ppm]	140Ce [ppm]	141Pr [ppm]	146Nd [ppm]	147Sm [ppm]	153Eu [ppm]	157Gd [ppm]	159Tb [ppn
082815-1A	7.773132314	39.17739063	109.0%	102.1%	35.59644151	80.15033772	9.867416869	38.63113225	8.48232198	1.845169499	8.19868952	1.21860523
082815-1B	2.046146708	10.76852703	108.9%	103.6%	7.788678373	19.18759309	2.386248413	9.343848509	2.156753888	0.296239327	2.046957999	0.29640529
082815-1C	4.478218036	25.74657904	110.2%	105.5%	15.40090937	36.78465559	4.592720546	18.47845561	4.329096903	0.847212386	4.545922011	0.71878317
082815-1D	6.034947114	25.74221417	108.9%	104.3%	8.859103385	21.0544968	2.728419743	12.00047363	3.102880888	0.629493091	3.584297511	0.64801349
082815-2A	7.65570284	46.01544247	106.8%	104.4%	27.42444035	65.8186548	7.880917301	32.39444878	7.419940724	1.521115523	7.641817671	1.23665722
082815-2B	5.924885704	25.52450462	107.2%	105.0%	8.514909016	19.47931823	2.549311939	10.60613174	2.86945642	0.599621162	3.303320645	0.58503902
082815-3A	9.179586918	44.52777214	106.5%	106.1%	36.9493435	91.19792265	10.68768744	42.85422812	9.037624228	2.105892907	8.19582145	1.23109841
082815-3B	5.792991656	27.38559213	105.8%	105.4%	9.226902808	21.19594058	2.677174409	11.26314004	2.844908254	0.677449714	3.419695612	0.63586715
112215-A	8.505152975	28.18742277	104.9%	105.9%	37.33690869	81.54261877	9.439774081	36.18682052	6.663761438	1.62195961	5.743787729	0.8470068
112215-B1	12.1881518	30.45975463	102.4%	103.7%	48.143143	104.8025986	12.32592094	47.6936565	9.069515441	2.026140484	7.229652808	1.02119330
112215-B2	10.15730421	35.076209	100.9%	104.4%	44.4133236	98.46108754	11.64278108	45.68710499	8.993594254	2.022252697	7.631494172	1.09567099
112215-C1	1.548237898	10.12422958	95.7%	97.2%	11.43895148	27.82514698	2.820573462	10.68128838	2.160205833	0.389221034	1.9378284	0.28372919
12215-C2	1.319584189	10.03674682	94.4%	96.1%	10.15315428	25.30779045	2.528343577	9.940847308	1.947667797	0.38726597	1.920044211	0.28833048
112215-D	2.00507003	7.518489395	95.5%	98.5%	10.65253509	26.60335306	2.62273868	10.02763338	1.920920108	0.36991891	1.768658004	0.24500503
MK3	4.734134019	18.60269027	96.8%	100.2%	27.45688171	68.8198745	6.930165949	26.93322427	5.052796255	0.979773903	4.17238958	0.58852842
MK5B	6.328210958	25.11574569	93.2%	97.3%	33.31272789	72.7185237	8.706891022	33.81783304	6.820011767	1.515004009	5.887377854	0.83468284
MK6A	8.852111901	35.89302509	92.2%	95.8%	44.54241304	102.2735798	11.77839326	46.29238723	9.028397806	1.909972317	7.821628132	1.10266050
MK6	11.14811564	37.51829039	92.0%	95.8%	50.98261791	109.9445849	13.58913932	51.95032444	10.07678654	2.370962202	8.385348869	1.15298980

	163Dy [ppm]	165Ho [ppm]	166Er [ppm]	169Tm [ppm]	172Yb [ppm]	175Lu [ppm]	185Re	232Th ([ppm]	238U [ppm]
082815-1A	7.749111848	1.537477547	4.574653829	0.651853556	4.443420848	0.639036231	100.6%	5.692029221	2.285329911
082815-1B	2.011902333	0.394935065	1.544990344	0.188280922	1.48150608	0.224003196	106.0%	12.23790952	1.424509191
082815-1C	4.682958654	0.953883474	2.940108629	0.432104723	2.961607489	0.495435831	101.7%	5.352238803	1.765454206
082815-1D	4.612363974	1.036141359	3.292513998	0.50499734	3.666391355	0.601832619	102.3%	9.742772928	2.123222757
082815-2A	8.282539305	1.705604664	5.472043283	0.786973463	5.203234454	0.806873951	103.9%	8.404904992	2.792738156
082815-2B	4.291909972	0.927578061	3.103609614	0.445980973	3.497143641	0.510290431	106.2%	7.437669111	1.72010465
082815-3A	8.062011189	1.682258127	5.18254038	0.762649682	5.376419763	0.80617149	104.5%	7.226680771	2.603908778
082815-3B	4.486906214	1.027688274	3.258855863	0.517430001	3.620745315	0.560358857	103.3%	4.653325541	1.952457971
112215-A	5.310416058	1.076976108	3.412215618	0.50310632	3.42484789	0.53352707	104.2%	9.95205716	2.642134471
112215-B1	6.011712076	1.184919057	3.576815987	0.522073573	3.539187012	0.536276523	105.3%	11.49173746	2.771377611
112215-B2	6.799602797	1.353447273	4.024282029	0.611336704	4.027870532	0.610954348	102.8%	12.81830351	3.442472661
112215-C1	1.802929199	0.355082996	1.158605622	0.152049744	1.151011326	0.172408543	102.9%	2.524553165	0.787035291
12215-C2	1.839236291	0.373921568	1.159132471	0.164732513	1.188703199	0.178544809	99.9%	2.222911323	0.808405791
112215-D	1.471906431	0.272939913	0.877122241	0.129218879	0.958666998	0.147607435	103.3%	2.325358195	0.857119696
MK3	3.426538924	0.6926249	2.158293943	0.334134201	2.322831908	0.37832643	101.7%	5.399308727	2.072266444
MK5B	4.847282429	0.918869675	3.30848915	0.424045938	3.018663482	0.478281831	100.0%	8.78787303	2.519614778
MK6A	6.635361678	1.318431201	4.027768478	0.594050201	4.283472528	0.675341444	100.4%	11.35356536	3.652702858
MK6	6.998314705	1.417596574	4.401146315	0.638102007	4.583239102	0.713668205	98.7%	13.3339886	3.13948573

XRF Analysis

	Na_2O(%)	MgO(%)	Al_2O_3(%)	SiO_2(%)	P_2O_5(%)	K_2O(%)	CaO(%)	TiO_2(%)	MnO(%)	Fe_2O_3(%)
082815-1A	0.116	0.905	14.252	69.211	0.171	9.695	0.43	0.63	0.004	4.631
082815-1B	ND	0.274	1.056	98.832	0.174	0.864	0.167	0.351	-0.002	0.585
082815-1C	ND	4.411	6.792	73.915	0.164	4.71	7.186	0.631	0.105	2.281
082815-1D	ND	3.188	3.298	85.121	0.198	2.504	4.934	0.754	0.131	1.619
082815-2A	ND	0.594	8.585	81.327	0.292	5.49	0.47	1.017	0.003	3.061
082815-2B	ND	4.926	3.455	79.828	0.205	2.326	7.709	0.633	0.194	1.834
082815-3A	ND	1.743	18.026	63.266	0.247	11.179	0.34	0.885	ND	3.708
082815-3B	ND	0.279	3.97	90.833	0.228	2.972	0.231	0.593	0.33	2.03
112215-A	0.257	0.775	17.65	66.231	0.133	11.055	0.456	0.933	0.018	2.114
112215-B1	ND	1.193	20.09	71.139	0.199	11.142	0.161	1.185	0.014	3.039
112215-B2	2.18	0.728	16.396	67.774	0.198	8.872	0.166	1.032	0.002	1.973
112215-C1	ND	0.114	1.981	98.383	0.172	1.554	0.161	0.226	ND	0.159
12215-C2	ND	0.109	1.736	97.333	0.15	1.49	0.161	0.254	0.005	0.162
112215-D	ND	0.09	1.555	98.098	0.164	1.129	0.161	0.252	0.003	0.259
MK3	-0.99	0.182	5.44	93.481	0.228	0.642	0.166	0.481	0.006	0.496
MK5B	ND	0.184	9.305	90.254	0.238	0.539	0.161	1.178	ND	0.166
MK6A	ND	0.475	12.44	84.061	0.217	1.645	0.184	1.094	0.012	1.201
MK6	ND	0.865	25.732	68.65	0.136	2.612	0.161	1.329	ND	0.774

XRD Analysis

	Formation	Quartz (%)	K-Feldspar (%)	Dolomite (%)	Muscovite (%)	Calcite (%)	Kaolinite (%)
082815-1A	Cm	69.9	-	8.8	3.4	-	-
082815-1B	Cm	89.1	-	7	-	0.2	-
082815-1C	Cm	30.2	-	24.1	-	-	-
082815-1D	Cm	74.1	-	24.9	-	-	-
082815-2A	Cm	40.3	13	0.6	-	0.7	-
082815-2B	Cm	57.1	25.4	35.1	-	-	-
082815-3A	Cm	13.8	50.6	0.6	30	0.4	-
082815-3B	Cm	16.2	23.6	0.6	-	0.7	-
112215-A	Cdh	28.4	45.6	7.9	17.1	-	-
112215-B1	Cdh	25	-	9.1	51	2.2	-
112215-B2	Cdh	23.2	37.6	6.3	37.5	1.4	-
112215-C1	Cdh	67.3	6.8	-	-	-	-
112215-C2	Cdh	90.2	10.8	-	-	-	-
112215-D	Cdh	87.4	8.5	-	-	-	-
MK3	Cc	72.8	-	-	-	-	22.1
MK5B	Cc	75.7	-	-	-	-	37.7
MK6A	Cc	72.9	-	-	-	-	27.4
M6	Cc	24.6	-	-	12.4	-	68.2

WORKS CITED

1. Ayotte, J.D., Montgomery, D.L., Flanagan, S.M., Robinson, K.W., 2003, Arsenic in groundwater in eastern New England: occurrence, controls, and human health implications: Environmental Science & Technology, v. 37 (10), p. 2075-2083.

2. Balan, E., Trocellier, P., Jupille, J., Fritsch, E., Muller, J., Calas, G., 2001, Surface chemistry of weathered zircons: Chemical Geology, v. 181 (1-4), p. 13–22.

3. Banning, A., Rüde, T. R., 2015, Apatite weathering as a geological driver of high uranium concentrations in groundwater: Applied Geochemistry, v. 59, p. 139-146.

4. Baturin, G. N., and Kochenov, A. V., 2001, Uranium in Phosphorites: Lithology and Mineral Resources, v. 36.4, p. 303-21. Translated from Litologiya i Poleznye Iskopaemye

5. Bean, Jared, ms, 2009, A Geochemical and Hydrogeological Analysis of Naturally-Occurring Radioactivity in Groundwater, Hinesburg, Vermont: Senior thesis: Middlebury College, Middlebury, Vermont, 67 p.

6. Bense, V., Gleeson, T., Loveless, S., Bour, O., & Scibek, J., 2013, Fault zone hydrogeology: Earth-Science Reviews, v. 127, p. 171-192.

7. Blatt, H., Middleton, G. V., and Murray, R. C., 1980, Origin of Sedimentary Rocks: Englewood Cliffs, NJ, Prentice-Hall.

8. Boggs, S. ,2001, Principles of Sedimentology and Stratigraphy: Upper Saddle River, NJ, Prentice Hall.

9. Deer, W. A., Howie, R. A. and Zussman, J., 1966, An Introduction to the Rock-Forming Minerals: New York, Wiley.

10. Dempster, T. J., Martin, J. C., Shipton, Z. K., 2008, Zircon dissolution in a ductile shear zone, Monte Rosa granite gneiss, northern Italy: Mineralogical Magazine, v. 72, p. 971–86.

11. Eaton, T.T., Anderson, M.P., and Bradbury, K.R., 2007, Fracture control of ground water flow and water chemistry in a rock aquitard: Ground Water, v. 45, p. 601-615.

12. EPA (2014). National Primary Drinking Water Regulations, online resource. Last accessed 11/19/15. http://water.epa.gov/drink/contaminants/

13. EPA (2015) [A]. How EPA Regulated Drinking Water Contaminants. Last accessed 12/11/15. http://www.epa.gov/dwregdev/how-epa-regulates-drinking-water-contaminants

14. EPA (2015) [B]. Private Well Owners. Last accessed 09/26/15. http://www.epa.gov/region1/eco/drinkwater/private_well_owners.html

15. EPA (2015) [C]. Table of Regulated Drinking Water Contaminants. Last accessed 12/11/15. http://www.epa.gov/your-drinking-water/table-regulated-drinking-water-contaminants

16. Faure, G., 1998, Principles and Applications of Geochemistry, 2nd Ed. London: Prentice Hall. 600 p.

17. Favorito, Julia, ms, 2014, An analysis of the lithologic control on major elements, radionuclides, and other trace elements in groundwater south of Bristol, Vermont: Senior Thesis, Middlebury College, Middlebury, Vermont.

18. Fetter, C.W., 2001, Applied Hydrogeology Fourth Edition: Prentice Hall, New Jersey.

19. Filoon, John, ms, 2012 A Hydrologic, Structural and Cartographic Analysis of Groundwater in the Vicinity of the Hinesburg Thrust, West-Central Vermont: Senior Thesis, Middlebury College, Middlebury, Vermont.

20. Grive, M., Grandia, J., Merino, L., Duro, L., and Bruno, J., 2007, Modeling of radium- barium sulphate co-precipitation in the near field of a HLNW repository: Goldschmidt Conference Abstracts, Spain.

21. Grundl, T., and Cape, M., 2006, Geochemical Factors Controlling Radium Activity in a Sandstone Aquifer: Ground Water Journal, v. 44(4), p. 518-527.

22. Kim, J., and Becker, L., 2001, Geologic context of elevated radionuclide occurrences in NW Vermont: NEGSA Abstracts.

23. Kim, J., Ryan, P., Klepeis, K., Gleeson, T., North, K., Bean, J., Davis, L. and Filoon, J., 2014, Tectonic evolution of a Paleozoic thrust fault influences the hydrogeology of a fractured rock aquifer, northeastern Appalachian foreland: Geofluids, v. 14, p. 266-290.

24. Langmuir, D., 1997, Aqueous Environmental Geochemistry: Upper Saddle River, New Jersey, Prentice-Hall, Inc.

25. McDonald, Emily, ms, 2012, A Model for Uranium Occurrence in the Late Cambrian Clarendon Springs Formation: Implications for Groundwater Quality in Northwestern Vermont: Senior Thesis, Middlebury College, Middlebury, Vermont.

26. Nesse, W. D., 2000, Introduction to Mineralogy: New York City, Oxford University Press.

27. Nichols, Andrew. L, ms, 2001, Mineralogical Evidence for a Hydrothermal Origin of the Brandon Residual Formation and the East Monkton Kaolins: Senior Thesis, Middlebury College, Middlebury, Vermont.

28. North, Katherine, ms, 2005, An Evaluation of Geologic Controls on Elevated Naturally-Occurring Radioactivity in Bedrock Ground Water Wells, Northwest Vermont: Senior Thesis, Middlebury College, Middlebury, Vermont.

29. Ogden, D.G., 1969, Geology and origin of the kaolin at East Monkton, Vermont: Economic Geology No. 3., Department of Water Resources, Montpelier, Vermont, p. 1-39.

30. Ratcliffe, N. M., Stanley, R. S., Gale, M. H., Thompson, P. J., 2011, Bedrock Geologic Map of Vermont: U.S. Geological Survey Scientific Investigations Map 2184, scale 1:100,000.

31. Reimann, C. and de Caritat, P., 1998, Chemical Elements in the Environment: Factsheets for the Geochemist and Environmental Scientist, New York: Springer-Verlag.

32. Ryan, P.C., Kim, J.J., Mango, H., Hattori, K., Thompson, A., 2013, Arsenic in a fractured slate aquifer system, New England (USA): Influence of bedrock geochemistry, groundwater flow paths, redox and ion exchange: Applied Geochemistry, v. 39, p. 181-192.

33. Seaton W., and Burbey T., 2000, Aquifer characterization in the Blue Ridge physiographic province using resistivity profiling and borehole geophysics: geologic Analysis: Journal of Environmental and Engineering Geophysics, v. 5, p. 45–58.

34. Senior, L.A. and Vogel, K.L., 1995, Radium and radon in ground water in the Chickies Quartzite, Southeastern Pennsylvania: U.S. Geological Survey Water-Resources Investigations Report 92-4088.

35. Shapiro, A.M., 2002, Fractured-rock aquifers: understanding an increasingly important source of water: United States Geological Survey Fact Sheet 112-02.

36. Stanley, R. S., 1980, Mesozoic faults and their environmental significance in western Vermont: Vermont Geological, v. 1, p. 22–32.

37. Vengosh, A., Hirschfeld, D., Vinson, D., Dwyer, G., Raanan, H., Rimawi, O., Al-Zoubi, A., Akkawi, E., Marie, A., Haquin, G., Zaarur, S., Ganor, J., 2009, High Naturally Occurring Radioactivity in Fossil Groundwater from the Middle East: American Chemical Society, v. 43(6), p. 1769–1775.

38. Vermont Department of Environmental Conservation: Drinking Water and Groundwater Protection Division, 2003. Well Completion Report Searchable

Database. Last accessed 04/04/2016. https://anrweb.vt.gov/DEC/WellDrillerReports/Default.aspx

39. Vermont Department of Health (2014). Manganese in Drinking Water. Last accessed 12/11/2015. http://healthvermont.gov/enviro/water/documents/manganese_fs.pdf

40. Vermont Department of Health (2015) [A] . Alpha Radiation. Last accessed 09/20/15. http://healthvermont.gov/enviro/rad/alpha.aspx

41. Vermont Department of Health (2015) [B] . Arsenic in Drinking Water. Last accessed 09/30/15. http://healthvermont.gov/enviro/water/arsenic.aspx

42. Vermont Geological Survey (2003). Geology of the Monkton Area, Vermont. Last accessed 10/06/15. http://www.anr.state.vt.us/dec/geo/MonktonMainEdit.htm

43. Woodhead, J. A., Rossman, G. R., Silver, L. T., 1991, The Metamictization of Zircon: radiation Dose-Dependent Structural Characteristics: American Mineralogist, v. 76, p. 74–82.

44. Zhang, T., Gregory, K., Hammack, R. W., Vidic, R. D., 2014, Co-precipitation of Radium with Barium and Strontium Sulfate and Its Impact on the Fate of Radium during Treatment of Produced Water from Unconventional Gas Extraction. Environmental Science & Technology, v. 48 (8), p. 4596-4603.